An alternative wood pyrolysis model based on TGA and cone calorimeter tests

Mariam Abdo, Hassan Flity, Lucas Terrei, André Zoulalian, Rabah Mehaddi, Pierre Girods, Yann Rogaume

An alternative wood pyrolysis model based on TGA and cone calorimeter tests

Mariam ABDO[a,b,c], Hassan FLITY[b], Lucas TERREI[b], André ZOULALIAN[a], Rabah MEHADDI[b], Pierre GIRODS[a], Yann ROGAUME[a]

[a] *Université de Lorraine, INRAE, LERMAB, ERBE, F-88000 Epinal, France*
[b] *Université de Lorraine, CNRS, LEMTA, F-54000, Nancy, France*
[c] *Fonte Flamme, 63100 Clermont Ferrand, France*

Abstract

Understanding the process of pyrolysis is crucial to achieve continuous progress in the efficient use of wood as a fuel source in various applications. In the literature, a wide range of kinetic models for wood pyrolysis has been introduced, varying from simpler to more complex and predictive. Some of these models are mathematical, with the sole objective of fitting the experimental results. The others are physical models that describe the underlying chemical processes involved in wood thermal degradation, but they tend to be more complex and time-consuming. In our study, a compromise between these two categories of models was established. A new physical and simple kinetic model of wood thermal degradation was proposed. This model was validated using a multi-scale approach. At micro scale, the thermal degradation of wood was studied using thermogravimetric analysis (TGA). TGA experiments were conducted with two wood species, beech and spruce, in an inert atmosphere at five different heating rates. Based on the latter analysis, our kinetic model of wood thermal degradation was established. Its associated kinetic parameters were determined by fitting the experimental mass loss and mass loss rate data. Good agreement was achieved between the experimental and numerical results. At bench scale, tests were performed in a controlled atmosphere chamber placed in front of a cone calorimeter. The thermal degradation of wood was studied at two heat fluxes in an inert atmosphere obtained by a constant argon injection. The kinetic model developed at the micro scale was implemented into a one-dimensional pyrolysis model, taking into account both thermal and mass transfer phenomena within the wood. The validity of the 1D pyrolysis model was established by comparing the numerical results with the mass loss, mass loss rate, and temperature profile measured during cone calorimeter tests.

Keywords: Wood, Pyrolysis, Thermogravimetric analysis, Kinetic, Cone calorimeter, Modelling

1. Introduction

Biomass is currently the world's largest renewable energy source, providing a scalable, flexible and, in many instances, the only reliable source of energy [1]. The term "biomass" commonly refers to all organic materials derived from plants, with wood being the primary type. For many years, wood has been employed

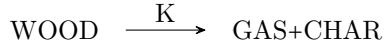

Figure 1: One step global reaction mechanism.

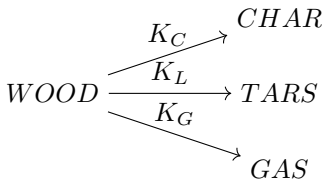

Figure 2: Independent competitive reactions scheme proposed by Shafizadeh and Chin [11].

mainly to cook food, heat space and satisfy the construction needs of buildings, works of art and furniture [2]. Today, the sustainable production of heat and energy from wood is at the centre of scientific and industrial interest. Actually, the proper use of wood energy as a substitute for fossil fuels can have a particular impact on climate change by reducing the net release of carbon into the atmosphere [1] through sequestration in biomass and long-lived products. On the other hand, wood energy can also have an economic advantage by satisfying the growing demand for energy. The question is, how can wood energy be used sustainably to achieve these benefits?

For this purpose, research has aimed to characterise the pyrolysis, gasification and combustion of wood in order to design efficient and environmentally sustainable units. However, an accurate study of these techniques requires a global understanding of their fundamental processes, especially the primary pyrolysis phase. Pyrolysis, the thermal degradation of wood, is a potentially useful thermochemical conversion process. It is considered not only as an independent process for the production of bio-oil and biochar, but also as a first step of the gasification and combustion processes [3]. Therefore, knowledge of the wood pyrolysis behaviour, especially as a function of wood sample size, provides the quantitative basis for a general rigorous modelling approach applicable to any wood application in any scale [4, 5].

Many researchers have studied the thermal degradation behaviour of wood using thermogravimetric analysis (TGA). At this scale, small particles are used to ensure the absence of internal heat and mass transfer. The results obtained from TGA tests are used to determine reaction mechanisms and kinetic data of wood pyrolysis. In the literature, numerous kinetic schemes for wood pyrolysis have been carried out. Many authors [6, 7, 8] have considered a one-step global reaction that converts wood to volatile products and char without a detailed description, as shown in Fig .1. Other authors such as Caballero *et al.* [9] and Thunman *et al.* [10] have used kinetic schemes with independent competitive reactions. These schemes follow the proposal of Shafizadeh-Chin [11] shown in Fig. 2.

Multi-stage mechanisms were also used in the literature [12, 13, 14, 15], suggesting the presence of intermediate components as shown in Fig. 3. Furthermore, there are many authors who consider that the description

Nomenclature

α_{abs}	Average absorptivity [-]	K_0	Pre-exponential factor [s^{-1}]
Δh	Reaction heat [$J \cdot kg^{-1}$]	m_0	Initial mass [Kg]
λ	Thermal conductivity [$W \cdot m^{-1} \cdot K^{-1}$]	Cp	Thermal capacity [$J \cdot kg^{-1} \cdot K^{-1}$]
$q_e^{"}$	External heat flux per unit area [$kW \cdot m^{-2}$]	E	Activation energy [$kJ \cdot mol^{-1}$]
$q_{loss}^{"}$	Heat losses per unit area [$kW \cdot m^{-2}$]	h	Thermal convective coefficient [$W \cdot m^{-2}$]
$Q_r^{"}$	sum of reaction heat [$kW \cdot m^{-2} \cdot K^{-1}$]	L	Thickness of the sample [m]
ρ	Density [$kg \cdot m^{-3}$]	R	Universal gas constant [$J \cdot mol^{-1} \cdot K^{-1}$]
σ	Stefan-Boltzman constant [$W \cdot m^{-2} \cdot K^{-4}$]	T	Temperature [K]
ε	Emissivity [-]	t	Time [s]
K	reaction rate [s^{-1}]	x	Distance from the exposed surface [m]

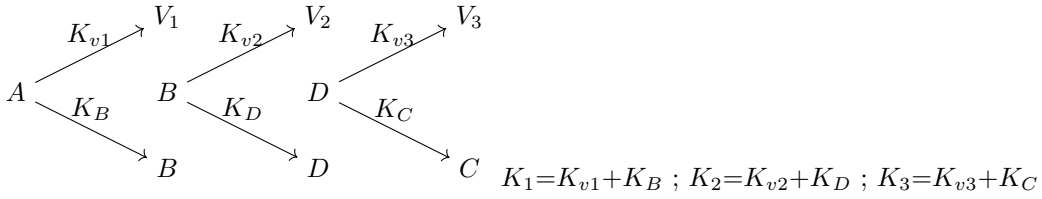

Figure 3: Multi-stage pyrolysis mechanisms proposed by Di Blasi and Branca [14] (A is the wood, B and D are intermediate components).

of wood pyrolysis with only one component is not accurate enough. For instance [16, 17, 18, 19, 20, 21] assumed that the wood pyrolysis is the sum of its main components: cellulose, hemicellulose and lignin. This reaction scheme, shown in Fig. 4, can be applied to a variety of wood species, as the content of cellulose, hemicellulose and lignin varies from one type of wood to another. A major disadvantage of this reaction scheme is that it neglects the interactions between the different components and ignores the influence of minerals. Table 1 summarises the main mechanisms of wood/biomass pyrolysis in the literature. A wide variation in the kinetic parameters can be observed in the literature. At a first glance, it appears that the degradation reactions of lignocellulosic material are more commonly assumed to be first-order reactions. The activation energy of the one-component reaction presents widely variable values, roughly comprised between

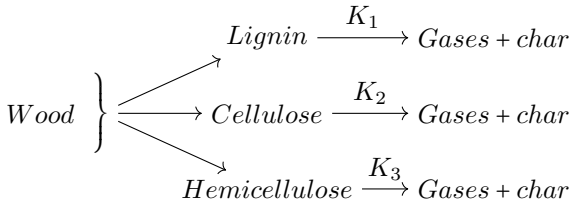

Figure 4: Independent parallel reactions model.

44 and 243 $kJ \cdot mol^{-1}$. Likewise, the activation energies vary between 86 and 147 $kJ \cdot mol^{-1}$ for hemicellulose, 193 and 236 $kJ \cdot mol^{-1}$ for cellulose, and 46-181 $kJ \cdot mol^{-1}$ for lignin. This variation may be due to the large variability of the biomass resource, the operating conditions and the mathematical treatment of the experimental data. The variation observed in this context may also be ascribed to the compensation effect of Arrhenius parameters. Changes in the activation energy (E_a) could be partly or entirely offset by adjustments in the pre-exponential factor or reaction order, and conversely [22, 23].

Table 1: Summary of one-component and multi-component mechanisms of lignocellulosic material pyrolysis.

Reaction mechanism	Author (Ref.)	Biomass	Experimental system	Size/mass	Reaction order	Kinetic constants: E ($kJ \cdot mol^{-1}$), A (s^{-1})
Fig.1	Tang *et al.* [6]	Ponderosa Pine	Dynamic TGA 325-350 °C	20-100 mg	1	K= 6.5×10^{6} exp (226/RT)
Fig.1	Thurner and Mann [7]	Oak	Isothermal tube furnace 300-400 °C	650 μg	1	K=2.47×10^{6} exp (106.5/RT)
Fig.1	Wagenear *et al.* [8]	Pine	Isothermal TGA 380 °C	100-125 μg	1	K=1.4×10^{10} exp (150/RT)
Fig.2	Font *et al.* [9]	Olive stones	Dynamic TGA 2, 10 and 25 $K \cdot min^{-1}$	3-4 mg	1.58	k_G=1.27×10^{13} exp (163.4/RT)
					0.667	k_L= 4.3×10^{13} exp (194.6/RT)
					7.21	k_C=6.59×10^{16} exp (188.1/RT)
Fig.2	Thunman *et al.* [10]	Pine	Pyrex reactor	-	1	k_G=1.3×10^{8} exp (140/RT)
					1	k_L= 2.0×10^{8} exp (133/RT)
					1	k_C=1.08×10^{7} exp (121/RT)
Fig.3	Wared and Braslaw [12]	Lignin	Isothermal TGA 300 °C	0.25mm	1	k_1=9.6×10^{8} exp (186.73/RT)
					1	k_2= 1.57×10^{16} exp (205.9/RT)
					1	k_3=1.13×10^{17} exp (240/RT)
Fig.3	Miller and Bellan [13]	Cellulose	Isothermal tube furnace 300-450 °C	≤ 80 μg	1	k_1=2.8×10^{19} exp (242.4/RT)
					1	k_2= 3.28×10^{14} exp (196.5/RT)
					1	k_3=1.3×10^{10} exp (150.5/RT)
Fig.3	Di blasi and Branca [14]	Beech	Isothermal tube furnace 300-450 °C	≤ 80 μg	1	k_1= 2.7×10^{4} exp (76.2/RT)
					1	k_2=5.9×10^{9} exp (142.8/RT)
					1	k_3=9.97 exp (43.8/RT)
Fig.3	Di blasi and Branca [15]	Beech	Dynamic TGA 5, 10, 20, 40 $K \cdot min^{-1}$ from the initial temperature to 500 °C	5 mg	1	k_1= $6.29\times 10'$ exp (106/RT)
					1	k_2=8.6×10^{17} exp (226/RT)
					1	k_3=7.83×10^{6} exp (114/RT)
					1.54	k_3=1.10×10^{12} exp (183/RT)
Fig.4	Gronli *et al.* [18]	Birch	Dynamic TGA 5 $K \cdot min^{-1}$ from the initial temperature to 500 °C	5 mg	1	$k_{Hemicellulose}$= 7.96×10^{2} exp (100/RT)
					1	$k_{Cellulose}$=4.06×10^{7} exp (236/RT)
					1	k_{Lignin}=1.8 exp (46/RT)
Fig.4	Branca *et al.* [19]	Beech	Dynamic TGA 5, 20, 80 $K \cdot min^{-1}$ from the initial temperature to 500 °C	20 mg	1	$k_{Hemicellulose}$= 2.527×10^{11} exp (147/RT)
					1	$k_{Cellulose}$=1.379×10^{14} exp (193/RT)
					1	k_{Lignin}=2.202×10^{12} exp (181/RT)
Fig.4	Barneto *et al.* [21]	Rice straw pulp	Dynamic TGA 5, 10, 20 $K \cdot min^{-1}$ from the initial temperature to 500°C	10-100 mg	1	$k_{Hemicellulose}$= 2.19×10^{9} exp (86/RT)
					1	$k_{Cellulose}$=1.17×10^{15} exp (206/RT)
					1	k_{Lignin}=8.97×10^{2} exp (62/RT)

For coarse or "thermally thick" wood samples, the internal gradients cannot be neglected. In this case, the chemistry of thermal decomposition is influenced by heat and mass transfer effects. It is therefore necessary to take into account in the modelling process the complex nature of wood, the coupling between chemical kinetics, heat transfer and mass transfer that takes place during the pyrolysis process of solid samples. Many efforts, both experimental and theoretical [24, 25, 26, 27], have been carried out to better understand the complex mechanisms interacting in the thermal degradation of thermally thick wood samples. Among all these researchers, many authors have studied the thermal degradation of wood at the cone calorimeter scale. Most of these studies have been carried out in an oxidative atmosphere [28, 5, 29, 30, 31, 32, 33, 34]. Under these conditions, oxidation reactions involving the gases (flame) and carbon (smouldering) increase the complexity of the problem. Therefore, it is necessary to limit these reactions and pay attention to pyrolysis by working in an inert atmosphere. Whereas, the study of wood degradation at the cone calorimeter in an inert atmosphere has been a subject of few prior investigations. In this area, the experimental study of Kashiwagi *et al.* [35] has for many years been the basis of numerous numerical works to develop a pyrolysis model. This study provides experimental data on mass loss rates and information on the in-depth temperatures for two heat fluxes: 25

and 40 $kW \cdot m^{-2}$. Swann *et al.* [36], on the other hand, has developed a new apparatus, Controlled Atmosphere Pyrolysis Apparatus II, which facilitates the collection of data on mass loss rate, temperature, and sample shape for materials exposed to radiant heating in a controlled atmosphere. However, this apparatus has not been applied in the study of wood pyrolysis. Lautenberger and Fernandez-Pello [37], Jia *et al.* [38] and Richter *et al.* [39] used data from Kashiwagi *et al.* [35] to validate their thermal pyrolysis model. Stoliarov *et al.* [40] proposed a specific calculation code, Thermakin, to investigate the thermal degradation of polymer materials. This code allows the analysis of the decomposition of various types of materials in different dimensions, ranging from 0D to 2D. Terrei *et al.* [41] have performed a new experimental setup allowing to study the wood thermal degradation at the cone calorimeter scale in an inert atmosphere. This study provides experimental data on mass loss rates and in-depth temperatures of spruce wood for three heat fluxes: 38, 49 and 59 $kW \cdot m^{-2}$. These measurements were used to validate their one-dimensional pyrolysis model with GPYRO [41]. More recently, Gong and Yang [42] have published an exhaustive review regarding the pyrolysis of commonly used solid combustibles.

In summary, wood pyrolysis has been investigated using a multiscale approach in the literature. In this approach, relatively simplified schemes are preferred to avoid lengthy calculation times. Numerous kinetic models, ranging from simpler to more complex and predictive, have been introduced in previous studies. Some of these models are mathematical, with the sole objective of fitting the experimental results. The others are physical models that describe the underlying chemical processes involved in wood thermal degradation, but they tend to be more complex and time-consuming. However, the ongoing challenge lies in formulating a simple kinetic model capable of accurately predicting mass loss and mass loss rate data while maintaining fidelity to the underlying chemical processes involved in wood thermal degradation. The present work addresses this challenge at the micro scale. At the bench scale, several wood pyrolysis models are available in the literature. However, the properties of these models are calibrated to fit the experimental data. In most cases, the large number of unknown properties in the model and the limited amount of experimental data result in non-intrinsic properties. Therefore, when the experimental setup is changed or scaled up, the reliability of the model decreases. This aspect is the main focus of this paper at a larger scale.

A global multi-reaction kinetic model of wood thermal degradation was proposed. This model was inspired from a two stages, semi global multi reaction kinetic model established to study the carbonisation of olive wood [43]. It divides the wood into three pseudo-components that are not considered to be the main components of wood: hemicellulose, cellulose and lignin. These pseudo-components degrade in a single step reaction, which allows a proper study of the kinetic aspects related to a variable temperature levels. The best set of the model kinetic parameters is then determined by an optimisation method. A comparison between numerical and experimental evolutions of the mass loss and the mass loss rate for the different heating rates obtained

from TGA showed a good agreement. At larger scale, cone calorimeter tests were then carried out in an inert atmosphere at two heat fluxes (38 and 49 $kW \cdot m^{-2}$). Mass loss and in-depth temperatures at twelve different positions were measured. A 1D-pyrolysis model was developed by coupling the kinetic model with the mass and energy consevation equations. All the properties of the model were taken from literature or determined through experimental measurements, except for the thermal conductivity above 200 °C. This particular property was estimated by fitting the mass loss data obtained from cone calorimeter tests. To validate the model at this scale, an additional experiment was conducted using a different heat flux of 25 $kW \cdot m^{-2}$, which was not used to optimize the model parameters. The latter model shows good efficiency in predicting the experimental results obtained from the cone calorimeter tests.

2. Study at the micro scale

This section presents the experimental and numerical studies conducted at the micro scale to evaluate the thermal degradation of wood in an inert atmosphere, with a primary focus on chemical aspects. Two wood species, beech and spruce, were used for the tests. These species have chemical compositions representative of the typical standards for the hardwood and softwood categories, respectively [15].

2.1. Thermogravimetric analysis

The degradation studies were performed using a STA 449 f3 Jupiter thermobalance in an inert atmosphere of nitrogen at a flow rate of 20 $mL \cdot min^{-1}$. The tests were conducted using approximately 50 ± 3 mg of wood powder with a thickness of less than 0.1 mm. Before each test, the samples were dried at 105 °C for 24 hours to remove moisture. During the experiments, the sample was heated from the ambient temperature to 800 °C at five different heating rates of 5, 10, 20, 30 and 40 $K \cdot min^{-1}$. The mass of the wood sample and the furnace temperature were continuously recorded. For each experiment, mass loss and normalised mass loss rate curves were plotted as a function of temperature. The mass loss represents the ratio of the sample weight (m) to the initial weight (m_0). The normalised mass loss rate curves were obtained numerically using the time derivative of the mass loss curves. In order to ensure good reproducibility of the experiments, at least two runs were carried out for each heating rate. Therefore, the reported experimental data correspond to the average of these tests, where the relative difference was less than 2 %.

Fig. 5a and Fig. 5b show the mass loss curves, for beech and spruce wood, respectively, under nitrogen atmosphere at five different heating rates 5, 10, 20, 30, 40 $K \cdot min^{-1}$. As can be seen in Fig. 5, the evolution of mass loss for both woods is similar regardless the heating rate. Even if the beech and spruce samples were pre-dried, the mass loss curves show a minor decline in mass before reaching 150 °C. This decrease is attributed to the evaporation of bound water still present in the wood. It is important to note that oven

drying at 105 °C can only remove free water and not bound water from the wood samples. Furthermore, about 70 % of the initial mass of beech and 65 % of the initial mass of spruce was found to be degraded between 240 and 400 °C, while 10 % of the initial mass of beech and 20 % of the initial mass of spruce was lost between 400 °C and 800 °C. The mass of the residue remaining at the end of the experiment was approximately 19 % and 21 % of the initial mass for beech and spruce, respectively. The analysis of Fig. 5 does not allow to clearly identify all the steps of the thermal degradation of beech and spruce wood under inert atmosphere. In this sense, Fig. 6a and Fig. 6b show the normalised mass loss rate curves, for beech and spruce wood respectively at five different heating rates 5, 10, 20, 30, 40 $\mathrm{K \cdot min^{-1}}$ under nitrogen atmosphere. For both woods, it was noticed that the pyrolysis process is characterised by two regions: main devolatilization and continuous slight devolatilization. The main pyrolysis process develops from about 240 °C to 400 °C at low heating rates (5, 10 and 20 $\mathrm{K \cdot min^{-1}}$) and 430 °C at high heating rates (30 and 40 $\mathrm{K \cdot min^{-1}}$). In this region, there are two peaks: a peak of approximately 305 °C at low heating rate and 350 °C at high heating rates. This peak is mainly related to hemicellulose decomposition. Another peak was observed at a higher temperature around 345 °C for low heating rates and 380 °C for high heating rates and is essentially related to the cellulose decomposition. The continuous slight devolatilization region occurred above 430 °C. This region corresponds to the slow degradation of lignin, which decomposes in both regions without characteristic peaks [44].

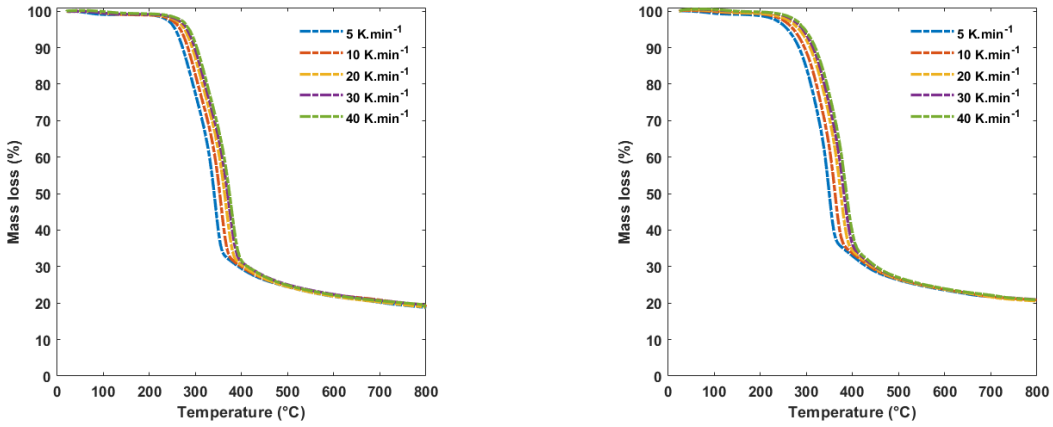

(a) Beech (b) Spruce

Figure 5: Normalised mass loss of beech and spruce wood in nitrogen atmosphere at five heating rates with TGA.

In order to quantify the effect of the heating rate on the degradation process characteristics of beech and spruce wood, the same parameters as those introduced by Gronli *et al.* [18] were evaluated and reported in Table 2. The initial degradation temperature $\mathrm{T}_{initial}$ was considered to be the temperature at which the solid mass fraction is equal to 0.975. The parameter T_{final} was obtained when the normalised mass loss rate curve represents an inflection point at a temperature of about 400 °C. The temperature of the first peak was

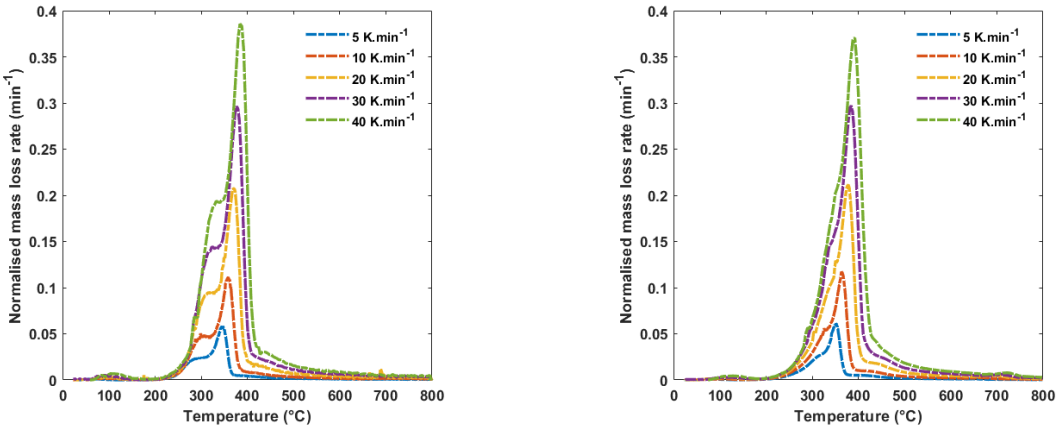

(a) Beech (b) Spruce

Figure 6: Normalised mass loss rate of beech and spruce wood in nitrogen atmosphere at five heating rate with TGA.

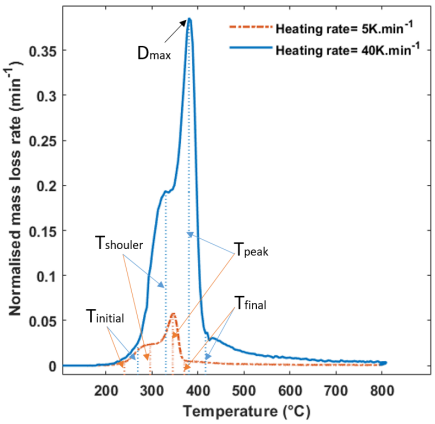

Figure 7: Normalised mass loss rate of beech with characteristic temperature for rates of 5 and 40 $\mathrm{K \cdot min^{-1}}$.

defined as $\mathrm{T}_{shoulder}$. The temperature T_{peak} was the temperature at which the maximum peak is reached. The maximum normalised mass loss rate was called D_{max}.

As the heating rate increased from 5 $\mathrm{K \cdot min^{-1}}$ to 40 $\mathrm{K \cdot min^{-1}}$ for beech and spruce wood, all the characteristic temperatures ($\mathrm{T}_{initial}$, T_{final}, $\mathrm{T}_{shoulder}$, T_{peak}) became successively higher especially $\mathrm{T}_{shoulder}$ and T_{peak}, as shown in Table 2. The whole decomposition process was shifted towards higher temperatures and the normalised mass loss rate increases. The shift of the normalised mass loss rate curves at higher temperature is clearly shown, for example, by the normalised mass loss rate curves of beech wood for 5 and 40 $\mathrm{K \cdot min^{-1}}$ reported in Fig. 7. The maximum normalised mass loss rate D_{max} showed an increasing trend up to about 0.39 $\mathrm{min^{-1}}$ for both species as the corresponding temperature increased from 342 °C to 380 °C for beech and from 350 °C to 392 °C for spruce wood. This can be interpreted on the basis of heat transfer limitations. Indeed, at a low heating rate, the sample has more time to establish a uniform temperature within it. On

the other hand, at a high heating rate, the sample has less time to establish a uniform temperature within it: heat transfer within the sample takes time, and the temperature at the core of the wood is not exactly the same as that of the reactor. In such a case, the kinetic aspect competes with the heat exchange aspect within the sample [45]. Therefore, the low heating rate results were used to evaluate the kinetic parameters for a proposed model. In this case, the temperature gradients in the samples are smaller and the process is controlled by the kinetics.

The mass loss and normalised mass loss rate curves for beech and spruce wood at the heating rate of 5 $\mathrm{K \cdot min^{-1}}$ are shown in Fig. 8a and Fig. 8b, respectively. It can be seen that the evolution of mass loss is similar for both woods and they differ only in the mass of the residue remaining at the end of the experiment. The normalised mass loss rate of beech shows a clear shoulder peak in the first stage of the normalised mass loss rate curve at around 300 °C, which is not obviously noticeable in the normalised mass loss rate curve of spruce, possibly due to its lower hemicellulose content compared to beech [18]. However, the differences in the corresponding degradation characteristics for beech and spruce at different heating rates are not exceedingly large. The characteristic parameters are quantitatively similar for both cases at different heating rates, as shown in Table 2. It is therefore worth looking for a common pyrolysis mechanism.

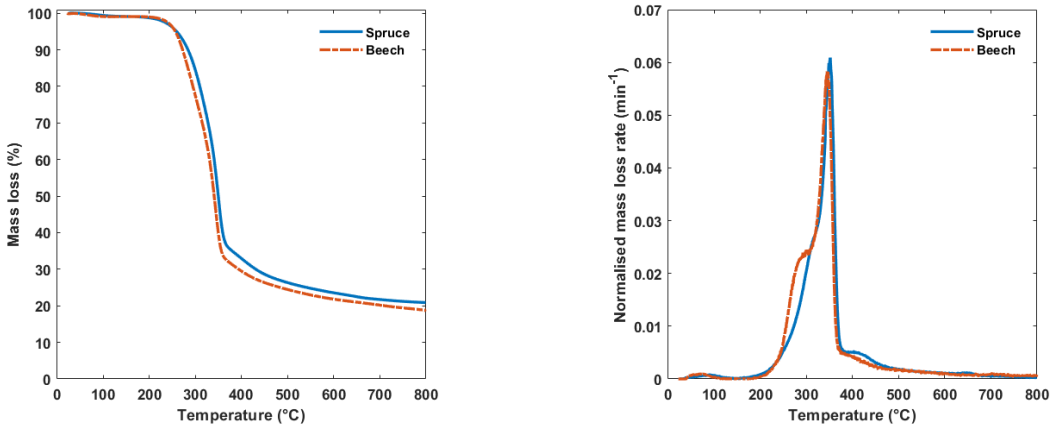

(a) Normalised mass loss

(b) Normalised mass loss rate

Figure 8: Mass loss and normalised mass loss rate curves of beech and spruce under a heating rate of 5 $\mathrm{K \cdot min^{-1}}$.

2.2. Kinetic model

As mentioned in the introduction, several kinetic models for the thermal degradation of wood have been proposed in the literature. Some describe the pyrolysis of wood in terms of a single component, while others recommend dividing the wood into three components corresponding to the main components of wood (hemicellulose, cellulose and lignin). Models of these two categories have advantages and drawbacks: more or less complex, more or less predictive. However, the thermal degradation of wood cannot be considered as

Table 2: Degradation characteristics parameters under different heating rate of beech and spruce wood.

Sample	Heating rate ($K \cdot min^{-1}$)	$T_{initial}$ (°C)	T_{final} (°C)	$T_{shoulder}$ (°C)	T_{peak} (°C)	D_{max} (min^{-1})
Beech	5	240	371	296	342	0.06
	10	249	387	300	357	0.11
	20	256	397	320	368	0.2
	30	263	412	331	374	0.29
	40	269	420	337	380	0.39
Spruce	5	234	380	317	350	0.06
	10	250	390	325	363	0.12
	20	260	407	342	376	0.2
	30	271	424	346	382	0.29
	40	277	430	350	392	0.4

a reflection of the sum of the thermal responses of its main components, since some inorganic components catalyse the conversion process in an unpredictable variety of ways [46, 47]. Furthermore, the interaction between the main components cannot be neglected, as shown by Hosoya *et al.* [48].

Based on the experimental results and on previous works, it was proposed to develop a global multi-reaction kinetic model of wood degradation in order to properly follow the kinetic aspects related to the variable temperature levels received by the sample. The model developed here is inspired from a two-stages, semi global multi-reaction kinetic model established to study the carbonisation of olive wood [43] and then used to study the isothermal degradation of wood panel and of its components [49].

In the proposed model, wood is divided into three pseudo-components A_1, A_2 and A_3. These pseudo solids cannot be assimilated to the main components, which are cellulose, hemicellulose and lignin. Each pseudo-component corresponds to a specific kinetic law and a mass fraction α_1, α_2 and α_3, respectively of the initial solid. A_1, A_2 and A_3 degrade in a single stage reaction to give gas products G_1, G_2 and G_3, respectively, and a non-degradable solid residue C_2 and C_3. It is worth mentioning that there is no chemical difference between C_2 and C_3. At low temperatures (T ≤ 300°C) only the degradation of A_1 occurs and the product is gaseous. Above this temperature, the transformation of the two pseudo-components A_2 and A_3 begins, giving gaseous products G_2 and G_3 and non-degradable solids C_2 and C_3 respectively. The proposed kinetic scheme is as follows:

$$\mathrm{A_1(First\ pseudo\ component)} \xrightarrow{k_1} \mathrm{G_1(Gas)}$$

$$\mathrm{A_2(Second\ pseudo\ component)} \xrightarrow{k_2} \mathrm{G_2(Gas)} + \gamma_2.\mathrm{C_2(Solid)}$$

$$\mathrm{A_3(Third\ pseudo\ component)} \xrightarrow{k_3} \mathrm{G_3(Gas)} + \gamma_3.\mathrm{C_3(Solid)}$$

γ_2 and γ_3 correspond to the mass fractions of solid produced by the components A_2 and A_3 respectively. K_i is the rate coefficient which follows an Arrehiuns-type law (K_i=K_{0i}.exp(-E_i/RT)). Assuming that the kinetics of the three reactions are described by first order laws, the mass balance of the solid and slightly volatile A_1, A_2, A_3, C_2 and C_3, can be respectively written as:

$$\frac{dm_{A1}}{dt} = -K_1.m_{A1} \tag{1}$$

$$\frac{dm_{A2}}{dt} = -K_2.m_{A2} \tag{2}$$

$$\frac{dm_{A3}}{dt} = -K_3.m_{A3} \tag{3}$$

$$\frac{dm_{C2}}{dt} = \gamma_2.K_2.m_{A2} \tag{4}$$

$$\frac{dm_{C3}}{dt} = \gamma_3.K_3.m_{A3} \tag{5}$$

The total mass of the sample at the time t, is then described by m(t), which is:

$$m(t) = m_{A1}(t) + m_{A2}(t) + m_{A3}(t) + m_{C2}(t) + m_{C3}(t) \tag{6}$$

The analytical resolution of the balance equations leads to the following equation:

$$\frac{m(t)}{m_0} = \gamma_2.\alpha_2 + \gamma_3.\alpha_3 + \alpha_1.exp(-K_1.t) + \alpha_2.(1-\gamma_2).exp(-K_2.t) + \alpha_3.(1-\gamma_3).exp(-K_3.t) \tag{7}$$

Eq. 7 shows that the calculated mass of the sample according to this model during the thermal degradation in an inert atmosphere depends on 11 kinetic and stoichiometric parameters (α_1, α_2, α_3, E_1, E_2, E_3, K_{01}, K_{02}, K_{03}, γ_2 and γ_3). These parameters must be estimated as they cannot be measured or determined experimentally. In practice, the least squares method was used to find the set of parameters that minimises the total error E_{r1} (Eq. 8) and E_{r2} (Eq. 9) between the numerical and experimental mass loss and mass loss rate respectively:

$$E_{r1} = \sum_{i=1}^{X} \left(\mathrm{m}_{num}(i) - \mathrm{m}_{exp}(i)\right)^2 \tag{8}$$

$$E_{r2} = \sum_{i=1}^{X} \left(\mathrm{mlr}_{num}(i) - \mathrm{mlr}_{exp}(i)\right)^2 \tag{9}$$

Where m_{num} and m_{exp} are respectively the numerical and experimental mass loss of the samples, mlr_{num} and mlr_{exp} are respectively the numerical and experimental normalised mass loss rate of the samples, and X is the number of experimental points. The Levenberg-Marquardt algorithm was used in the optimisation. Initially,

the kinetic parameters provided by Grioui *et al.* [43] were utilized as a set of initial values for the estimation based on E_{r2} (Eq. 9). The resulting kinetic parameters were then used as initial values to minimize E_{r1} (Eq. 8). This iterative process was repeated multiple times to obtain the optimal set of kinetic parameters that effectively fit the mass loss and mass loss rate curves simultaneously. To avoid heat and mass transfer limitations, the optimization process excluded the use of high heating rates (30 and 40 $\mathrm{K \cdot min^{-1}}$). Instead, the optimization was performed for the slow heating rates: 5, 10, and 20 $\mathrm{K \cdot min^{-1}}$ simultaneously. Indeed, employing the parameter estimation procedure on multiple experiments conducted under diverse conditions, such as various heating rates, while utilizing the same kinetic model and parameters, helped to circumvent the compensation effect [15]. The values of the kinetic parameters, obtained for beech and spruce wood, and the deviations between numerical and experimental are listed in Table 3.

The order of the reactions was kept constant and equal to one (n=1). The introduction of higher order reactions in this model provides an excellent description of the experimental results. This was not done in accordance with the hypothesis that the reaction rate depends only on the amount of reactant present in the reactor [50]. The other parameters were estimated with constraints to ensure a successive degradation of the three components in the following order: A_1, then A_2, and finally A_3. The degradation of the first component, leading to the formation of gases, precedes that of the second and third components which lead to the formation of gases and char.

Details about the dynamics of the different pseudo-components and a comparison between predicted and measured mass loss and normalised mass loss rate at the three heating rates: 5, 10 and 20 $\mathrm{K \cdot min^{-1}}$ for beech and spruce wood are shown in Fig. 9 and Fig. 10, respectively. In the case of beech, the reaction of the first pseudo-component A_1, which was completely converted to gas, started at 250 °C and was completed at 300 °C approximately. The maximum mass loss rate of A_1 occurred between 290 °C and 320 °C depending on the heating rate. As the heating rate is higher, the maximum mass loss rate occured at a higher temperature as shown in the section 2.1. The decomposition of the second pseudo-component A_2, which leads to the formation of gas and non-degradable solid C_2, started at about 300 °C and was completed at about 400 °C. The maximum mass loss rate of A_2 was proceeded between 340 °C and 370 °C. The final pseudo-component, A_3, initiated its degradation into gas and C_3 at approximately 420°C and concluded around 650°C. The maximum mass loss rate of A_3 was between 500 °C and 600 °C. The char was completely obtained at about 650 °C. For spruce, the decomposition of the first pseudo-component A_1 started at about 230 °C and was completed at 300 °C. The maximum mass loss rate of A_1 rate occurred between 320 °C and 340 °C depending on the heating rate. The decomposition of the second pseudo-component A_2 started at about 300 °C and was accomplished at about 400 °C. The maximum mass loss rate of A_2 was attained between 350 °C and 370 °C. The last pseudo-component A_3 initiated to degrade at about 400 °C and was achieved at about 650 °C with

Table 3: Kinetic parameters estimated for the thermal degradation of beech and spruce wood.

Sample	Reaction	E ($kJ \cdot mol^{-1}$)	K_{0_i} (1/s)	α	γ	Mean NRMSE (%)
Beech	(1)	116	3.4×10^8	0.2	-	1.72
	(2)	155	5.52×10^{10}	0.55	0.08	
	(3)	80	2.37×10^2	0.25	0.63	
Spruce	(1)	105	2.1×10^7	0.16	-	1.21
	(2)	172	1.3×10^{12}	0.6	0.15	
	(3)	76.5	2.52×10^2	0.24	0.56	

a maximum mass loss rate between 500 °C and 600 °C. The char was fully formed at about 650 °C. As can be seen, the simulated mass loss and the normalised mass loss rate for both species show a good agreement with the experimental results for different heating rates. The performance of the kinetic mechanism was evaluated using the Normative Root Mean Squared Error (NRMSE), between the experimental and predicted mass loss, characterised by the following variable:

$$NRMSE(\%) = \frac{\sqrt{\frac{\sum_{i=1}^{X}(\mathrm{m}_{num}(i)-\mathrm{m}_{exp}(i))^2}{X}}}{\max\limits_{i=1\ldots X} \mathrm{m}_{exp}(i) - \min\limits_{i=1\ldots X} \mathrm{m}_{exp}(i)} \cdot 100 \tag{10}$$

For beech the total deviation for the mass loss curve is about 1.06, 1.4 and 2.7 % for 5, 10 and 20 $K \cdot min^{-1}$ respectively, leading to an average NRMSE of 1.72 %. For spruce, the overall deviation for the mass loss curve is about 1.26, 1.27 and 2.1 % for 5, 10 and 20 $K \cdot min^{-1}$ respectively, giving an average NRMSE of 1.21 %. For both species, the fit of the model to the experimental mass loss and mass loss rate curves was very good from the ambient temperature to 400 °C. At temperatures above 400 °C, there is a slight discrepancy between the experimental and simulated curves. This can be attributed to a delayed degradation of the third pseudo-component. In addition, at higher temperatures, many reactions are likely to dominate which are not described in detail in this model and which cause the discrepancy. The maximum peak of the mass loss rate is slightly underestimated. This can be attributed to the presence of heat transfer phenomena and the experimental procedures. In any case, the prediction by the present model is considered encouraging in terms of the validity of the model itself.

To validate the kinetic parameters obtained through optimisation, these parameters were employed to predict mass loss and mass loss rates at elevated heating rates of 30 and 40 $K \cdot min^{-1}$. Despite these two heating rates not being incorporated into the optimization process, the model demonstrates its efficacy in predicting experimental mass loss and normalised mass loss rates for beech and spruce wood, as shown in Fig. 11 and Fig. 12, respectively. Indeed, the NRMSE for beech is 3.3 % at 30 $K \cdot min^{-1}$ and 3.5 % at 40 $K \cdot min^{-1}$. For spruce, it is 2.7 % at 30 $K \cdot min^{-1}$ and 3.1 % at 40 $K \cdot min^{-1}$.

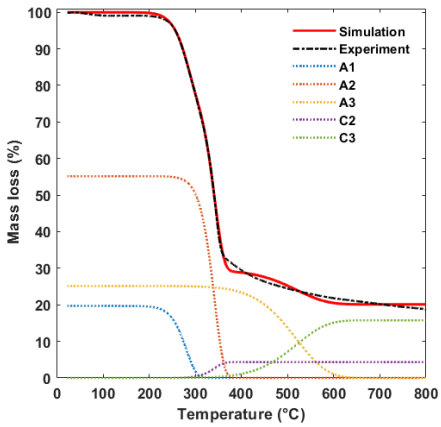

(a) 5 $\mathrm{K \cdot min^{-1}}$

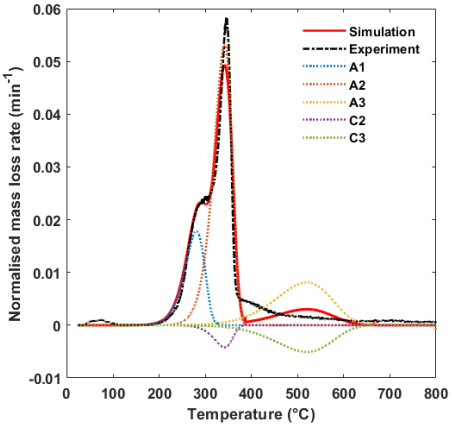

(b) 5 $\mathrm{K \cdot min^{-1}}$

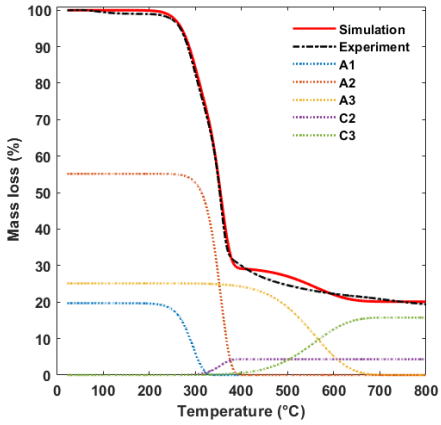

(c) 10 $\mathrm{K \cdot min^{-1}}$

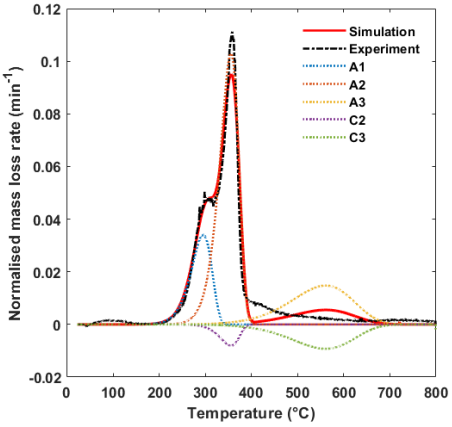

(d) 10 $\mathrm{K \cdot min^{-1}}$

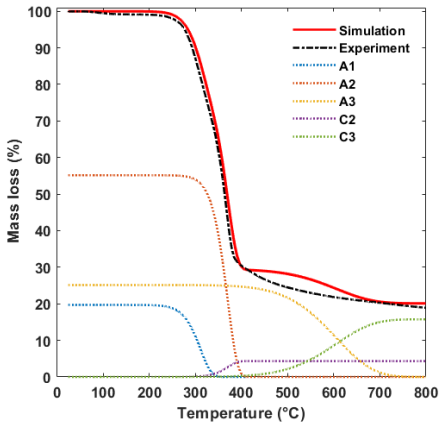

(e) 20 $\mathrm{K \cdot min^{-1}}$

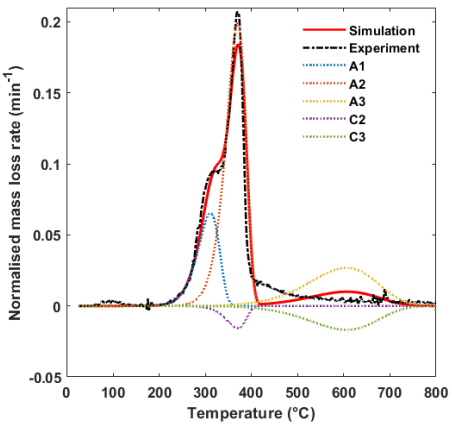

(f) 20 $\mathrm{K \cdot min^{-1}}$

Figure 9: Comparison between the experimental and the numerical mass loss and normalised mass loss rate curves for beech wood at 5, 10 and 20 $\mathrm{K \cdot min^{-1}}$.

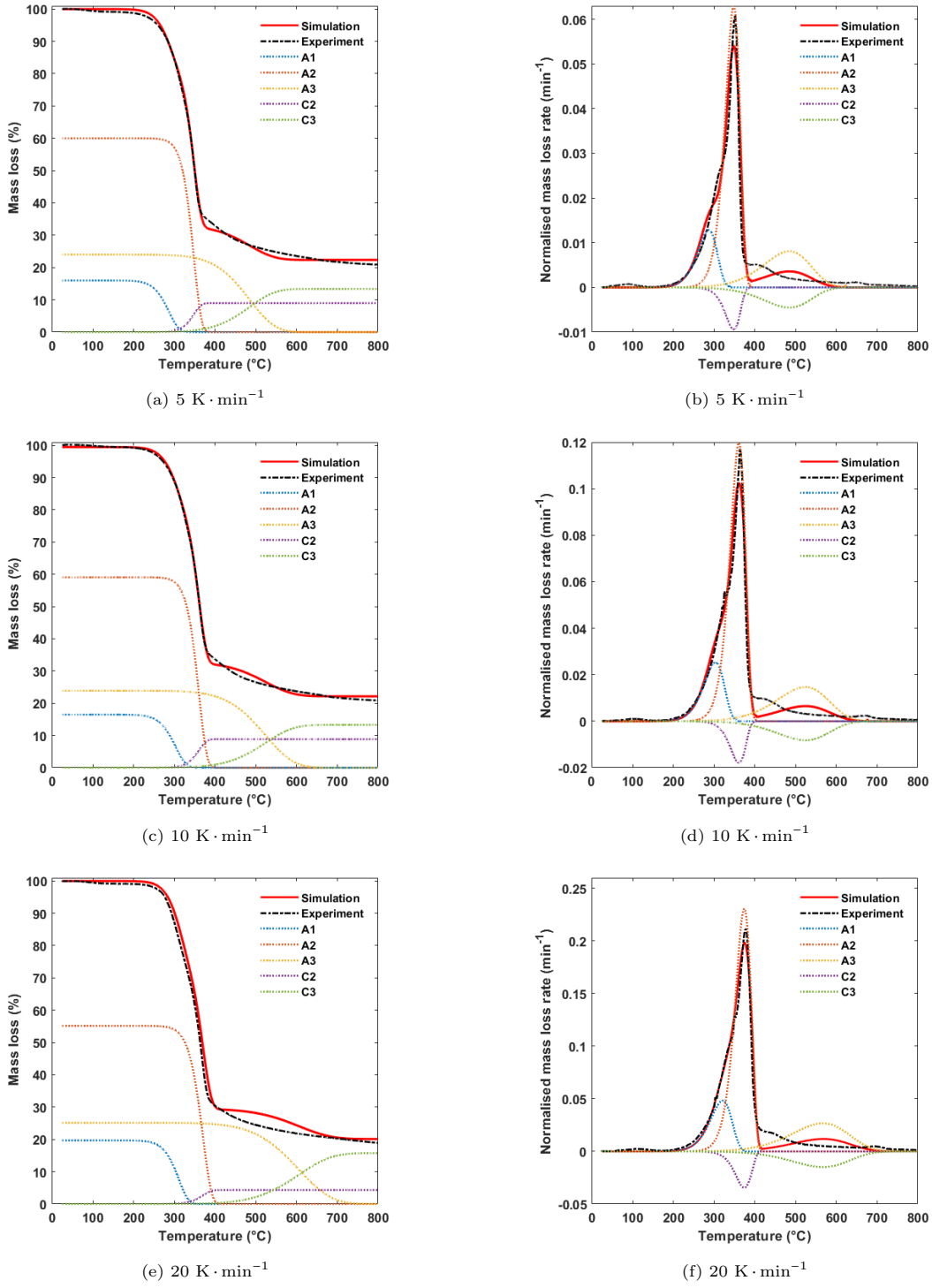

(a) 5 K · min^{-1}

(b) 5 K · min^{-1}

(c) 10 K · min^{-1}

(d) 10 K · min^{-1}

(e) 20 K · min^{-1}

(f) 20 K · min^{-1}

Figure 10: Comparison between the experimental and the numerical mass loss and normalised mass loss rate curves for spruce wood at 5, 10 and 20 K · min^{-1}.

3. Study at the bench scale

The objective of this section is to describe the thermal degradation of spruce and beech wood during the cone calorimeter experiments under inert atmosphere. First, the experiments performed at the cone

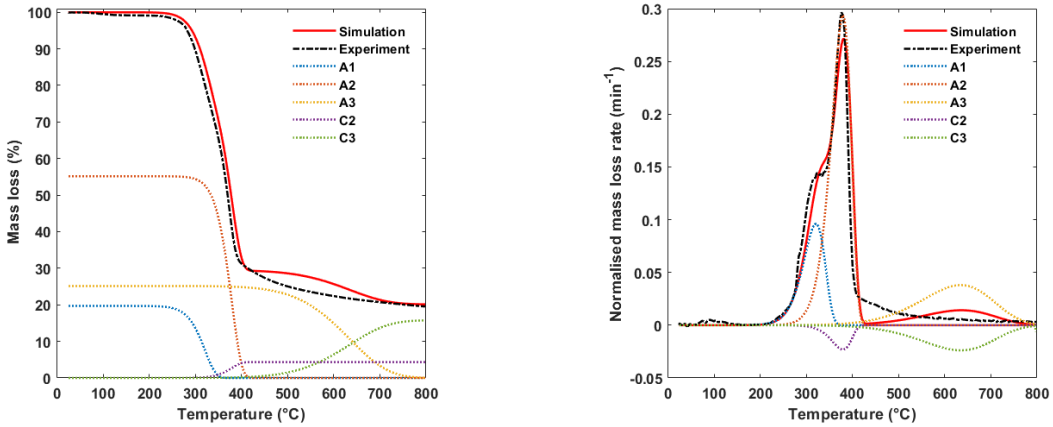

(a) 30 K · min^{-1}

(b) 30 K · min^{-1}

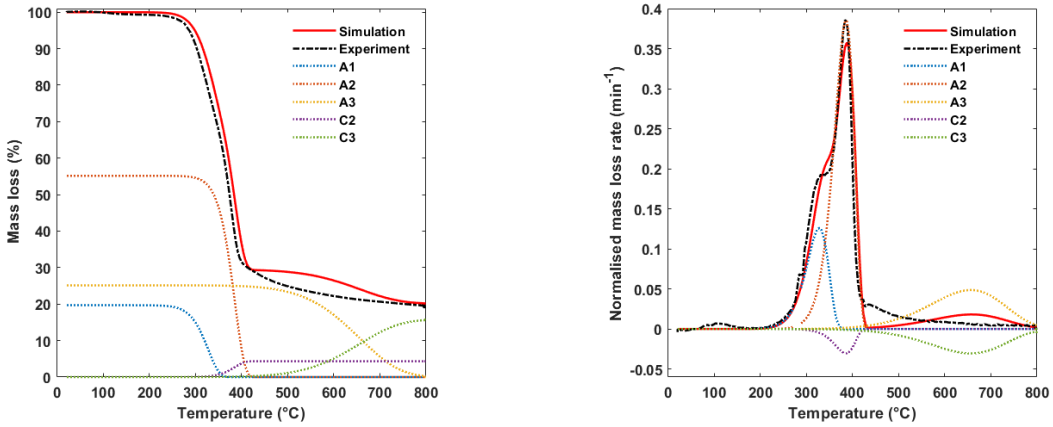

(c) 40 K · min^{-1}

(d) 40 K · min^{-1}

Figure 11: Comparison between the experimental and the numerical mass loss and normalised mass loss rate curves for beech wood at 30 and 40 K · min^{-1}.

calorimeter scale are briefly described. Then, the numerical model of pyrolysis at the cone calorimeter scale is presented.

3.1. Cone calorimeter experiments

As a detailed description of the experimental apparatus has been reported by Terrei *et al.* [41], only a brief description of the experimental setup is given here. The tests were performed in front of a cone calorimeter oriented vertically. During the tests, the sample was placed in a stainless-steel chamber specifically designed to study the wood thermal degradation under a controlled atmosphere. A sapphire window placed on the front face of the chamber allows the heat flux from the cone to pass through. The chamber was inerted by a continuous injection of argon at a flow rate of 10 L · min^{-1}. A Testo 350 gas analyser was used to determine the oxygen concentration. A test was started when the concentration of oxygen in the chamber stabilised at around 3 %. This concentration was always less than 6 % during the tests. For each test, the

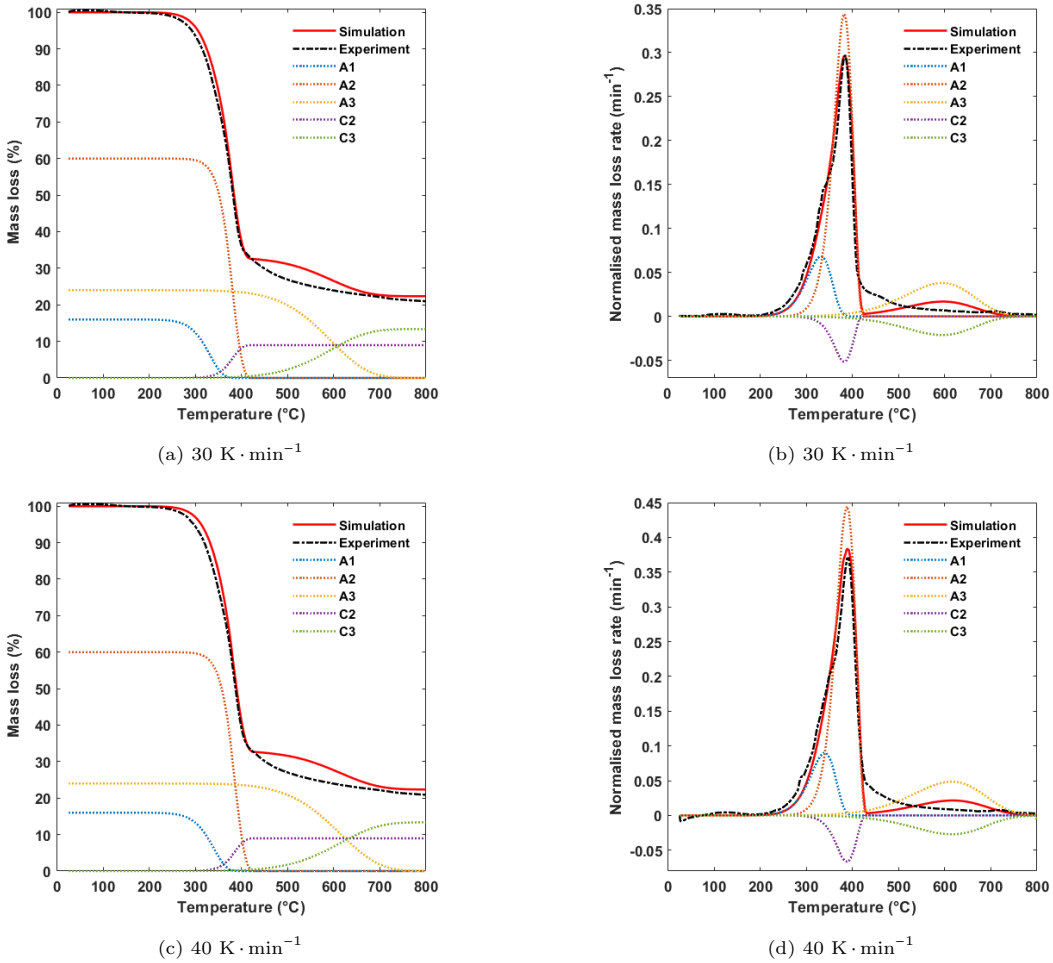

(a) 30 K · min^{-1}

(b) 30 K · min^{-1}

(c) 40 K · min^{-1}

(d) 40 K · min^{-1}

Figure 12: Comparison between the experimental and the numerical mass loss and normalised mass loss rate curves for spruce wood at 30 and 40 K · min^{-1}.

wood sample was placed in a specific sample holder made of low density calcium silicate plates to limit the thermal interactions with the edges and to ensure a 1-D heat transfer. The rear surface of sample is exposed to free gas flow. The sample and its holder were then inserted into the chamber via the rear face, which consists of a sliding door. Fig. 13 shows the experimental setup. The mass loss of the sample was measured using a load cell with a precision of 0.1 g. The in-depth temperatures were measured using twelve thin wire thermocouples embedded in the wood samples. Ten thermocouples were placed every 2 mm from 2 to 20 mm depth from the exposed surface, one at a 30 mm depth and one at a 40 mm depth. Tests were conducted at heat fluxes of 38 and 49 kW · m^{-2} for 10 minutes. The samples used in the tests were square wood samples of 100 × 100 × 50 mm^3, dried at 105 °C for 48 hours prior to each test to remove moisture. The initial mass of the samples tested was 180 ± 12 g and 300 ± 16 g for spruce and beech respectively. Terrei *et al.* [51] have already performed the tests only for spruce wood. In this study, the experimental data on spruce wood are identical to those presented in the study of Terrei *et al.* [51]. On the other hand, tests were carried out

using beech wood samples, with a few technical modifications. In these experiments, the flow rate of argon was 12 $L \cdot min^{-1}$ instead of 10 $L \cdot min^{-1}$ to ensure an oxygen concentration less than 3% throughout all the tests, and then to limit char oxidation as much as possible. In addition, a load cell with a precison of 0.01 g was used in order to provide a more reliable mass loss and mass loss rate. It is important to note that a single test was conducted on a spruce wood sample using a purging flow rate of 12 $L \cdot min^{-1}$. It was observed that the obtained mass loss rate is very similar to the mass loss rate obtained by Terrei et al. [51], who used a purging flow rate of 10 $L \cdot min^{-1}$.

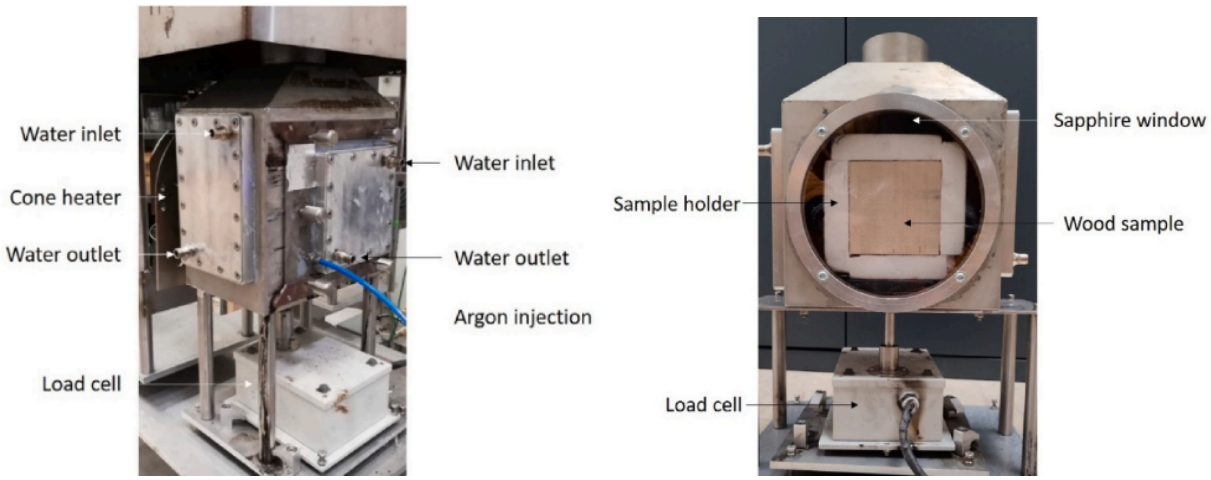

(a) (b)

Figure 13: (a) Back and (b) front side of the experimental setup [41].

3.2. Modeling of the cone calorimeter experiments

In the literature, many software have been used to simulate the degradation of wood at bench scale, like GPYRO, FDS and FireFoam. Previous works [52, 29] have shown the inadequacy of FDS to numerically simulate cone calorimeter tests with kinetic parameters calculated from TGA data. Otherwise, many authors [53, 39] have shown that GPYRO is able to well predict the thermal degradation behaviour of wood well. However, in GPYRO, the evolution laws of the model thermal properties are imposed. Regarding FireFoam, it is less commonly used in the literature compared to other software. In this paper, the modelling has been written in MATLAB® environment, in order to develop a model with a good knowledge of the assumptions and a good control of the evolution laws of all the properties. The modelling must focus on phenomena that can predict what happens inside the sample, such as heat transfer, mass transfer, chemical reactions, as well as the change in its thermophysical properties (conductivity, specific heat). The developed scheme and its associated kinetic parameter, validated at TGA scale, were used as input data to simulate the thermal decomposition of the spruce and beech wood at the cone calorimeter scale. The following assumptions were

made in the pyrolysis model:

1. The heat transfer was considered to be one dimensional since the wood sample seemed to degrade uniformly from the exposed side.
2. The heat and mass transfer between the solid and gas phases were neglected.
3. The thermo-physical properties of the three pseudo-components A_1, A_2, and A_3 were equivalent to those of dry wood.
4. The dimensions and shape of the wood sample remained constant and cracks and shrinkage were neglected.
5. The heat of the three chemical reactions was supposed to be the same and was taken from the literature [54].

Based on the above assumptions, the energy conservation equation for pyrolysis of the dry wood is described as:

$$\frac{\partial}{\partial t}\left[T(\rho_s C_{p_s})\right] = \frac{\partial}{\partial x}\left(\lambda_s \frac{\partial T}{\partial x}\right) + \mathrm{Q}_r^{"} \tag{11}$$

where: $\mathrm{Q}_r^{"}$ is the sum of reaction heat of the three pyrolysis reactions, as follows

$$\mathrm{Q}_r^{"} = k_1\alpha_1\rho_{A1}\Delta h_1 + k_2\alpha_2\rho_{A2}\Delta h_2 + k_3\alpha_3\rho_{A3}\Delta h_3. \tag{12}$$

Here, ρ_s is the bulk density described as the sum of the constituents (A_1, A_2 and A_3) and products (C_2 and C_3) densities as:

$$\rho_s = \alpha_1\rho_{A_1} + \alpha_2(\rho_{A_2} + \rho_{C_2}) + \alpha_3(\rho_{A_3} + \rho_{C_3}) \tag{13}$$

where, C_{p_s} and λ_s are respectively the thermal capacity and conductivity of the wood sample.

For the resolution of Eq. 11, it was assumed that at t=0, T=T_0, and that at t > 0, on the exposed side of the sample (x=0), the heat balance for the control volume with thickness (Δ_x) is as follows:

$$\left.\frac{\partial}{\partial t}\left[T(\rho_s C_{p_s})\right]\right|_{x=0} = \left(\alpha_{abs}\mathrm{q}_e^{"} - \mathrm{q}_{loss1}^{"} - \lambda_s \frac{\partial T}{\partial x}\right)/\Delta_x + \mathrm{Q}_r^{"} \tag{14}$$

where $\mathrm{q}_{loss1}^{"}$ is the heat balance of the control volume defined by:

$$\mathrm{q}_{loss1}^{"} = \sigma\varepsilon\left(\mathrm{T}_s^4 - \mathrm{T}_0^4\right) + h\left(\mathrm{T}_s - T_0\right) \tag{15}$$

Table 4: Values and correlations of thermophysical parameters used in the model.

Property	Correlation/Value	Ref.
Thermal conductivity ($\mathrm{W \cdot m^{-1} \cdot K^{-1}}$)	T<200 °C, λ_{spruce}= 0.102	Measured
	T >200 °C, $\lambda_{spruce} = 0.102 + 1.2 \cdot 10^{-6}(\mathrm{T} - 473)^2 + 3.7 \cdot 10^{-9}\,(T - 473)$	Optimised
	T<200 °C, λ_{beech}= 0.138	Measured
	T >200 °C, $\lambda_{beech} = 0.138 + 1.06 \cdot 10^{-6}(\mathrm{T} - 473)^2 + 6.42 \cdot 10^{-9}\,(T - 473)$	Optimised
Specific heat ($\mathrm{J \cdot kg^{-1} \cdot K^{-1}}$)	$C_{p_{wood}} = 1112 + 4.85 \cdot (T - 273)$	[55]
	$C_{p_{char}} = 808.9 + 0.93 \cdot (T - 273)$	[56]
Density ($\mathrm{kg \cdot m^{-3}}$)	ρ_{spruce}=360	Measured
	ρ_{beech}=600	Measured
Emissivity	ε=0.83	[41]
Convective coefficient ($\mathrm{W \cdot m^{-2} \cdot K^{-1}}$)	h=10	[57]
Absorptivity	$\alpha_{abs} = \varepsilon = 0.83$	[41]
Reaction heat ($\mathrm{kJ \cdot kg^{-1}}$)	$\Delta h_i = -100$	[54]

Moreover, for t> 0, at the back surface (x=L) another heat balance for the control volume with a thikness of (Δ_x) is established:

$$\frac{\partial}{\partial t}\left[T(\rho_s C_{p_s})\right]\Big|_{x=L} = \left(\lambda_s \frac{\partial T}{\partial x} - \mathrm{q}^{"}_{loss2}\right)/\Delta_x + \mathrm{Q}^{"}_r \tag{16}$$

where $\mathrm{q}^{"}_{loss2}$ is the heat losses by radiation and convection from the back surface and characterized by the following relation:

$$\mathrm{q}^{"}_{loss2} = \sigma\varepsilon\left(\mathrm{T}_b^4 - \mathrm{T}_0^4\right) + h\left(\mathrm{T}_b - T_0\right) \tag{17}$$

During wood pyrolysis, its thermo-physical properties such as thermal conductivity, specific heat, and density, change. The density of the sample was easily measured and then the variation in sample density was calculated by the model. The average initial density of the virgin spruce and beech samples was found to be 360 and 600 $\mathrm{kg \cdot m^{-3}}$ respectively. In contrast, it was difficult to obtain the variation of the thermal properties of wood (thermal conductivity and specific heat) over large temperature ranges (> 200 °C). In fact, above 200 °C, the properties of the original material are subjected to a large accompanying chemical reactions, and there are practical difficulties in determining material properties. Therefore, a wide range of different thermo-physical properties of wood were used in the literature. In addition, there is no clear trend in how the thermophysical properties vary in the modelling. Therefore, it was suggested that they should be chosen in such a way that the modelling results fit the experimental data well [24].

Fig. 14 shows the variations of the specific heat capacity of wood and char as a function of temperature reported in the literature. In most previous modelling studies, the heat capacity of wood and char were modelled as a linear function of temperature. In our case, the specific heat capacity of wood ($C_{p_{wood}}$) and char ($C_{p_{char}}$) was supposed to vary according to the relations of Wenzl *et al.* [55] and Anca-Couce *et al.* [56] respectively. The specific heat capacity of the wood sample was then assumed to vary linearly between wood and char depending on the conversion factor η, the ratio between the current and initial density ($C_{p_s} = (1 - \eta) \cdot C_{p_{wood}} + \eta \cdot C_{p_{char}}$). It is worth mentionning that the choice of the specific heat of wood and

char are not the most sensitive parameters affecting the accuracy of the model, as reported by Haberle [24]. For thermal conductivity, Di Blasi [25] in their extensive review on the modelling of chemical and physical

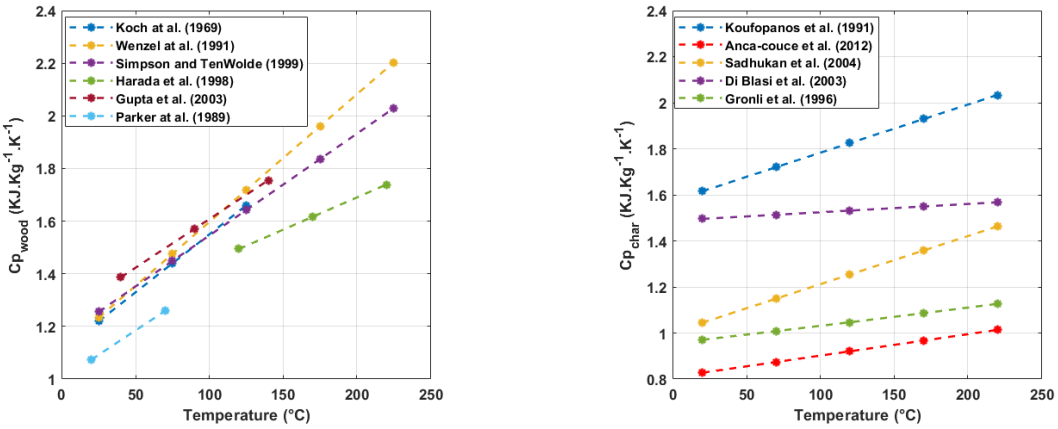

(a) Wood [58, 55, 59, 60, 61, 62]

(b) Char [63, 56, 64, 65, 66]

Figure 14: Specific heat capacities of wood and char available in literature.

processes of wood and biomass pyrolysis reported that among the wood properties, this property causes the highest sensitivity of the model predictions. In the literature, thermal conductivity was assumed to be mainly temperature dependent [60, 67]. In the present study, the thermal conductivity used was defined as follows:

1. Below 200 °C: the thermal conductivity of dry spruce and beech wood was measured in the laboratory using the hot wire method and was found to be 0.102 and 0.138 $\mathrm{W \cdot m^{-1} \cdot K^{-1}}$ respectively [68].
2. Above 200 °C: the thermal conductivity of spruce and beech was assumed to vary as a function of temperature as follows:

$$\lambda_{spruce} = 0.102 + a \cdot (\mathrm{T} - 473)^2 + b \cdot (T - 473) \tag{18}$$

$$\lambda_{beech} = 0.138 + c \cdot (\mathrm{T} - 473)^2 + d \cdot (T - 473) \tag{19}$$

Where a, b, c and d are four constants to be estimated. An inverse method was applied to the mass loss measurements obtained from the cone calorimeter tests at 38 and 49 $\mathrm{kW \cdot m^{-2}}$ simultaneously using this model. The Levenberg-Marquardt algorithm was used to minimise the following objective function:

$$E_r = \sum_{i=1}^{X} (\mathrm{m}_{num}(i) - \mathrm{m}_{exp}(i))^2 \tag{20}$$

Table 4 gives the thermal conductivity obtained by optimisation and the other properties used in the model. Fig. 15 shows the thermal conductivity of spruce and beech wood from the current study side by side with the available thermal conductivity from previous studies. For both species, the thermal conductivity increases with temperature, which is quite logical. The thermal conductivity of beech is higher than that of spruce,

which is quite satisfactory taking into account the difference in density between the two species. Fig. 15 also shows the large discrepancies in the thermal conductivity values used in the literature.

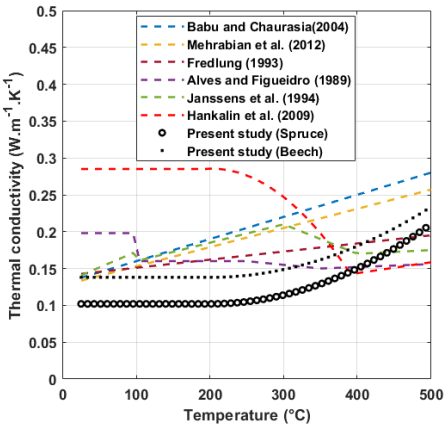

Figure 15: Thermal conductivity as a function of the temperature [69, 70, 71, 72, 73, 74].

Moreover, the emissivity of the wood surface was measured by Terrei *et al.* [41] and found to be 0.83. The value for the convective coefficient of the solid surface was taken as 10 $\mathrm{W \cdot m^{-2} \cdot K^{-1}}$ [57]. The heat and mass conservation equations were numerically solved using a finite volume method written in a MATLAB® code. The model allows the calculation of the temperature distributions within the sample, the mass loss and the mass loss rate per unit area (MLRPUA).

4. Results and discussion

This section presents the experimental and numerical results obtained at the cone calorimeter scale. Fig. 16 and Fig. 17 show the comparison between experimental and numerical temperatures at different depths within spruce and beech wood samples respectively during their decomposition in front of the cone calorimeter at 38 and 49 $\mathrm{kW \cdot m^{-2}}$. It can be noticed that the experimental and predicted in-depth temperatures are in good agreement for both species and heat fluxes. Although, the temperature predictions at depth (*i.e.* from 8 mm) were better than those near the surface. For 38 $\mathrm{kW \cdot m^{-2}}$, it can be seen that the calculated temperatures close to the surface for both species fit well the experimental data below 400 °C. Above this temperature, the simulation tends to underestimate the experimental evolution of near-surface temperatures. In contrast, the simulation predicts very well the temperature evaluation in large depths. For tests at 49 $\mathrm{kW \cdot m^{-2}}$, the simulation tends to slightly overestimate the experimental near-surface temperatures below 500 °C for both species. Beyond this value, the simulation underestimates the experimental data. As for 38 $\mathrm{kW \cdot m^{-2}}$, the model predicts very well the temperature evolution from 8 mm. In general, the numerical

results are in good agreement with the experimental results for low temperatures (< 350 °C). For higher temperatures, and especially near to the exposed surface, there is some bias. This bias mainly caused by the low accuracy of measurements during the conversion of wood into char. As the wood undergoes pyrolysis and transforms into char, its porosity increases, leading to decreased thermal contact between the material and the thermocouple. Additionally, the ignorance of the effects of the volume shrinkage and cracks in this model could also be another source of the bias. However, the numerical temperatures were quite satisfactory.

Fig. 18 and Fig. 19 present the comparison between the mass loss and the Mass Loss Rate Per unit Area (MLRPUA) as a function of the time obtained by the model and those obtained from experiments performed at 38 and 49 $\mathrm{kW \cdot m^{-2}}$ for spruce and beech wood respectively. It can be noticed that there is a good agreement between the calculated and the experimental results for both species, whatever the heat flux. The performance of the model was evaluated by calculating the NRMSE (Eq. 10), between the experimental and predicted mass loss. For spruce wood, the NRMSE is 1.5 and 3.8 % for 38 and 49 $\mathrm{kW \cdot m^{-2}}$ respectively. For beech wood, the NRMSE is 3.2 and 0.7 % for 38 and 49 $\mathrm{kW \cdot m^{-2}}$ respectively. Regarding the MLRPUA for both species, the numerical and experimental results are in good agreement for the quasi steady state. However, the numerical peak of the MLRPUA is overestimated at the beginning, especially for spruce. This bias may be due to an initial overestimation of temperatures from the near-surface thickness. To summarize, the model predict well the temperature profiles inside wood, the mass loss and the mass loss rate at the scale of the cone calorimeter. An additional experiment was conducted using a different heat flux of 25 $\mathrm{kW \cdot m^{-2}}$ with samples of spruce and beech wood. The results of this experiment were not used for optimising the model parameters. Instead, they were employed for model validation. The purpose of this experiment was to verify the predictive capability of the model and assess its performance when applied to conditions beyond those used for parameter optimisation. Fig. 20 shows the efficiency of the model in predicting mass loss and MLRPUA obtained from the experiments conducted at 25 $\mathrm{kW \cdot m^{-2}}$ for spruce and beech wood. For spruce, the NRMSE is 4.9 %, while for beech, it is 2.2 %. So, despite the results under a heat flux of 25 $\mathrm{kW \cdot m^{-2}}$ not being utilised for optimising the model parameters, the model demonstrates its efficiency in predicting experimental mass loss and normalised mass loss rates for beech and spruce wood under this flux.
These results validate the kinetic model developped at the micro scale in this study and show that the multi-scale approach is appropriate to model the wood pyrolysis at large scales.

5. Conclusion

In this work, the thermal degradation of beech and spruce wood has been investigated throughout the multi-scale approach. At the micro scale, the thermal degradation of spruce and beech wood was studied using a thermogravimetric analyser at five heating rates (5, 10, 20, 30 and 40 $\mathrm{K \cdot min^{-1}}$) under an inert

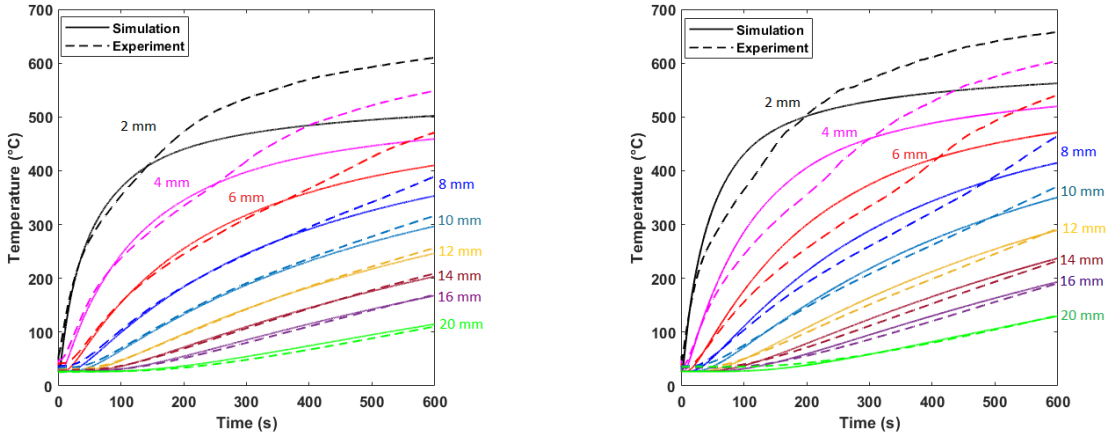

(a) 38 $\mathrm{kW \cdot m^{-2}}$ (b) 49 $\mathrm{kW \cdot m^{-2}}$

Figure 16: Comparison between the experimental and the numerical in-depth temperatures of spruce wood for 38 and 49 $\mathrm{kW \cdot m^{-2}}$ heat fluxes.

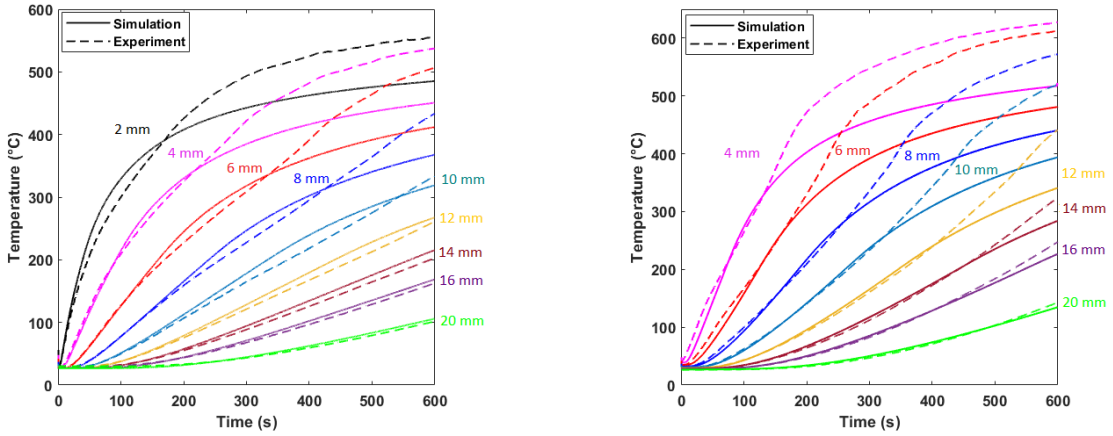

(a) 38 $\mathrm{kW \cdot m^{-2}}$ (b) 49 $\mathrm{kW \cdot m^{-2}}$

Figure 17: Comparison between the experimental and the numerical in-depth temperatures of beech wood for 38 and 49 $\mathrm{kW \cdot m^{-2}}$ heat fluxes.

atmosphere. The results led to a suggested wood thermal degradation mechanism with global multi-reactions. The associated kinetic parameters for both species were calculated by using the least squares method. The results showed efficient predictions in agreement with experimental mass loss and mass loss rate for different heating rates. At the bench scale, the model was completed by adding a heat and mass transfer model to the kinetic mechanism. At this scale, the model was validated by comparing the predicted results with those obtained from cone calorimeter tests. These tests were performed in a specific chamber, which was designed to perform tests in an inert atmosphere. The wood samples (beech and spruce) were exposed to three heat fluxes (25, 38 and 49 $\mathrm{kW \cdot m^{-2}}$) for 600 s. The results predicted by the model were in good agreement with the experimental measurements. Our perspective for the model developed in this study is to couple it

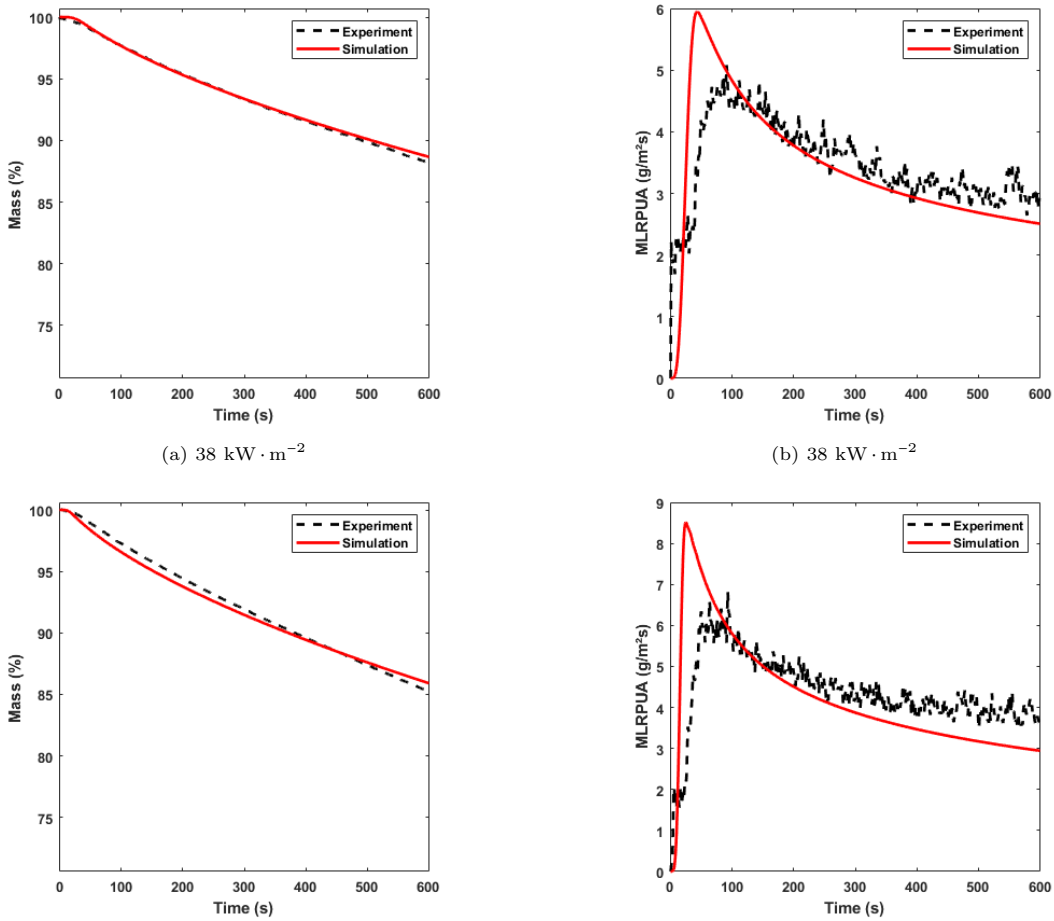

(a) 38 $\mathrm{kW \cdot m^{-2}}$

(b) 38 $\mathrm{kW \cdot m^{-2}}$

(c) 49 $\mathrm{kW \cdot m^{-2}}$

(d) 49 $\mathrm{kW \cdot m^{-2}}$

Figure 18: Comparison between the experimental and the numerical mass loss and MLRPUA for spruce wood for 38 and 49 $\mathrm{kW \cdot m^{-2}}$ heat fluxes.

with a kinetic model of char oxidation as a function of oxygen concentration in order to model the thermal degradation of wood in an oxidative atmosphere and at different intermediate oxygen concentrations.

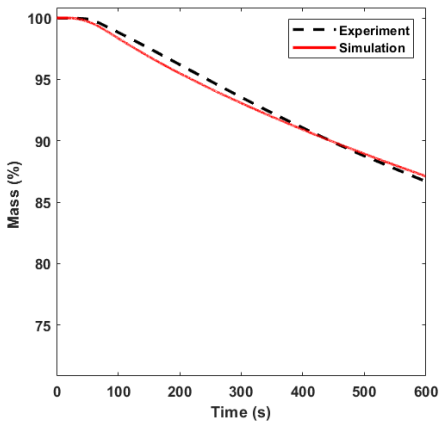

(a) 38 $\mathrm{kW \cdot m^{-2}}$

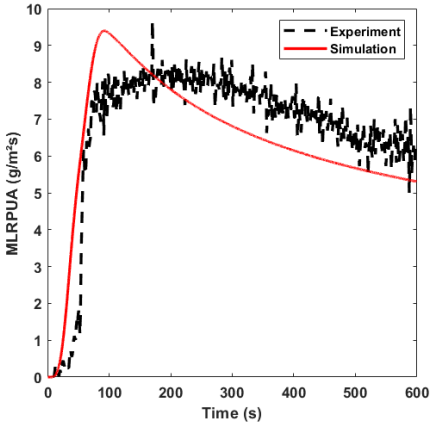

(b) 38 $\mathrm{kW \cdot m^{-2}}$

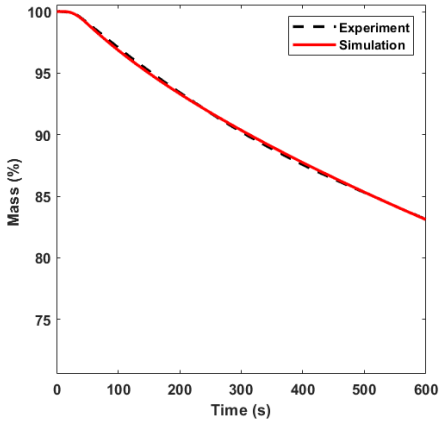

(c) 49 $\mathrm{kW \cdot m^{-2}}$

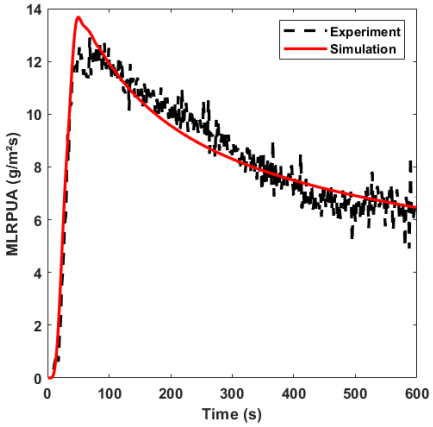

(d) 49 $\mathrm{kW \cdot m^{-2}}$

Figure 19: Comparison between the experimental and the numerical mass loss and MLRPUA for beech wood for 38 and 49 $\mathrm{kW \cdot m^{-2}}$ heat fluxes.

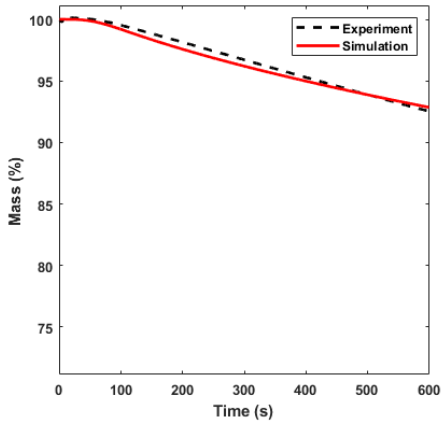

(a) Spruce

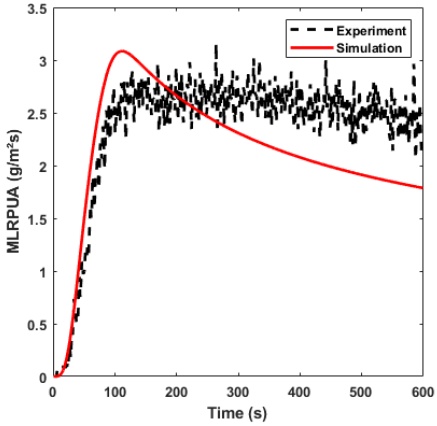

(b) Spruce

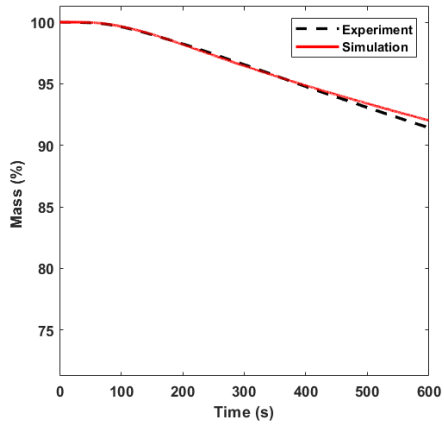

(c) Beech

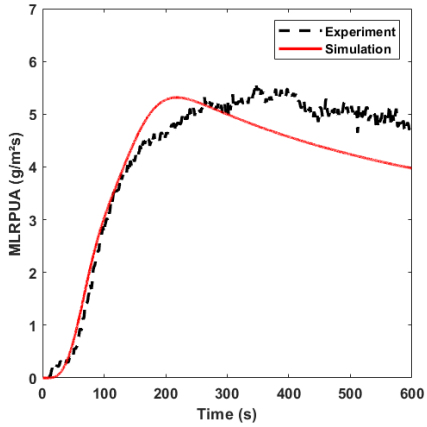

(d) Beech

Figure 20: Comparison between the experimental and the numerical mass loss and MLRPUA for spruce and beech wood for 25 $\mathrm{kW \cdot m^{-2}}$ heat flux.

References

[1] United Nations, Wood Energy in the ECE Region: Data, Trends and Outlook in Europe, the Commonwealth of Independent States and North America, UN, 2019. doi:10.18356/ca9e54f6-en.
URL https://www.un-ilibrary.org/content/books/9789213631096

[2] M. Simo-Tagne, M. C. Ndukwu, M. N. Azese, Experimental modelling of a solar dryer for wood fuel in epinal (france), Modelling—International Open Access Journal of Modelling in Engineering Science (2020).

[3] C. A. Koufopanos, A. Lucchesi, G. Maschio, Kinetic modelling of the pyrolysis of biomass and biomass components, Can. J. Chem. Eng. 67 (1) (1989) 75–84. doi:10.1002/cjce.5450670111.
URL https://onlinelibrary.wiley.com/doi/10.1002/cjce.5450670111

[4] C. Di Blasi, G. Russo, Modeling of Transport Phenomena and Kinetics of Biomass Pyrolysis, in: A. V. Bridgwater (Ed.), Advances in Thermochemical Biomass Conversion, Springer Netherlands, Dordrecht, 1993, pp. 906–921. doi:10.1007/978-94-011-1336-6_70.
URL http://link.springer.com/10.1007/978-94-011-1336-6_70

[5] W.-C. R. Chan, M. Kelbon, B. B. Krieger, Modelling and experimental verification of physical and chemical processes during pyrolysis of a large biomass particle, Fuel 64 (11) (1985) 1505–1513. doi:10.1016/0016-2361(85)90364-3.
URL https://linkinghub.elsevier.com/retrieve/pii/0016236185903643

[6] W. Tang, Effect of Inorganic Salts on Pyrolysis of Wood, Alpha-cellulose, and Lignin Determined by Dynamic Thermogravimetry, U.S. Forest Service research paper FPL, Forest Products Laboratory, 1967.
URL https://books.google.fr/books?id=vMtBJcPyMCQC

[7] F. Thurner, U. Mann, Kinetic investigation of wood pyrolysis, Ind. Eng. Chem. Process Des. Dev. 20 (07 1981). doi:10.1021/i200014a015.

[8] B. M. Wagenaar, W. Prins, W. van Swaaij, Pyrolysis of biomass in the rotating cone reactor: modelling and experimental justification, Chemical Engineering Science 49 (1994) 5109–5126.

[9] J. Caballero, J. Conesa, R. Font, A. Marcilla, Pyrolysis kinetics of almond shells and olive stones considering their organic fractions, Journal of Analytical and Applied Pyrolysis 42 (2) (1997) 159–175. doi:10.1016/S0165-2370(97)00015-6.
URL https://linkinghub.elsevier.com/retrieve/pii/S0165237097000156

[10] H. Thunman, B. Leckner, F. Niklasson, F. Johnsson, Combustion of wood particles—a particle model for eulerian calculations, Combustion and Flame 129 (1-2) (2002) 30–46. doi:10.1016/S0010-2180(01)00371-6.
URL https://linkinghub.elsevier.com/retrieve/pii/S0010218001003716

[11] F. SHAFIZADEH, P. P. S. CHIN, Thermal Deterioration of Wood, in: Wood Technology: Chemical Aspects, Vol. 43 of ACS Symposium Series, AMERICAN CHEMICAL SOCIETY, (1977), pp. 57–81, section: 5. doi:10.1021/bk-1977-0043.ch005.
URL https://doi.org/10.1021/bk-(1977)-0043.ch005

[12] S. Ward, J. Braslaw, Experimental weight loss kinetics of wood pyrolysis under vacuum, Combustion and Flame 61 (3) (1985) 261–269. doi:10.1016/0010-2180(85)90107-5.
URL https://linkinghub.elsevier.com/retrieve/pii/0010218085901075

[13] R. Miller, J. Bellan, A Generalized Biomass Pyrolysis Model Based on Superimposed Cellulose, Hemicelluloseand Liqnin Kinetics, Combustion Science and Technology 126 (1-6) (1997) 97–137. doi:10.1080/00102209708935670.
URL http://www.tandfonline.com/doi/abs/10.1080/00102209708935670

[14] C. Branca, C. D. Blasi, Kinetics of the isothermal degradation of wood in the temperature range 528–708 K, J. Anal. Appl. Pyrolysis (2003).

[15] C. Branca, C. Di Blasi, Global interinsic kinetics of wood oxidation, Fuel 83 (1) (2004) 81–87. doi:10.1016/S0016-2361(03)00220-5.
URL https://linkinghub.elsevier.com/retrieve/pii/S0016236103002205

[16] R. Radmanesh, Y. Courbariaux, J. Chaouki, C. Guy, A unified lumped approach in kinetic modeling of biomass pyrolysis, Fuel 85 (9) (2006) 1211–1220. doi:https://doi.org/10.1016/j.fuel.2005.11.021.
URL https://www.sciencedirect.com/science/article/pii/S0016236105004667

[17] G. Wang, W. Li, B. Li, H. Chen, Tg study on pyrolysis of biomass and its three components under syngas, Fuel 87 (4) (2008) 552–558, the 9th China–Japan Symposium on Coal and C1 Chemistry. doi:https://doi.org/10.1016/j.fuel.2007.02.032.
URL https://www.sciencedirect.com/science/article/pii/S0016236107001111

[18] M. G. Grønli, G. Várhegyi, C. Di Blasi, Thermogravimetric Analysis and Devolatilization Kinetics of Wood, Ind. Eng. Chem. Res. 41 (17) (2002) 4201–4208, publisher: American Chemical Society.

doi:10.1021/ie0201157.

URL https://doi.org/10.1021/ie0201157

[19] C. Branca, A. Albano, C. Di Blasi, Critical evaluation of global mechanisms of wood devolatilization, Thermochimica Acta 429 (2) (2005) 133–141. doi:https://doi.org/10.1016/j.tca.2005.02.030.

URL https://www.sciencedirect.com/science/article/pii/S0040603105001541

[20] R. Sharma, P. N. Sheth, A. M. Gujrathi, Kinetic modeling and simulation: Pyrolysis of jatropha residue de-oiled cake, Renewable Energy 86 (2016) 554–562. doi:https://doi.org/10.1016/j.renene.2015.08.066.

URL https://www.sciencedirect.com/science/article/pii/S0960148115302664

[21] A. G. Barneto, J. A. Carmona, J. E. M. Alfonso, R. S. Serrano, Simulation of the thermogravimetry analysis of three non-wood pulps, Bioresource Technology 101 (9) (2010) 3220–3229. doi:10.1016/j.biortech.2009.12.034.

URL https://linkinghub.elsevier.com/retrieve/pii/S096085240901699X

[22] J. Gong, L. Yang, A review on flaming ignition of solid combustibles: Pyrolysis kinetics, experimental methods and modelling, Fire Technology (2022) 1–98.

[23] L. Shi, C. Zhai, J. Gong, A method for addressing compensation effect in determining kinetics of biomass pyrolysis, Fuel 335 (2023) 127123.

[24] I. Haberle, . Skreiberg, J. Łazar, N. E. L. Haugen, Numerical models for thermochemical degradation of thermally thick woody biomass, and their application in domestic wood heating appliances and grate furnaces, Progress in Energy and Combustion Science 63 (2017) 204–252. doi:10.1016/j.pecs.2017.07.004.

URL https://linkinghub.elsevier.com/retrieve/pii/S0360128516301307

[25] C. Diblasi, Modeling chemical and physical processes of wood and biomass pyrolysis, Progress in Energy and Combustion Science 34 (1) (2008) 47–90. doi:10.1016/j.pecs.2006.12.001.

URL https://linkinghub.elsevier.com/retrieve/pii/S0360128507000214

[26] M. G. Groenli, A theoretical and experimental study of the thermal degradation of biomass (1996).

[27] R. Bilbao, J. Mastral, J. Ceamanos, M. Aldea, Modelling of the pyrolysis of wet wood, Journal of Analytical and Applied Pyrolysis 36 (1) (1996) 81–97. doi:https://doi.org/10.1016/0165-2370(95)00918-3.

URL https://www.sciencedirect.com/science/article/pii/0165237095009183

[28] A. K. Sadhukhan, P. Gupta, R. K. Saha, Modelling and experimental studies on pyrolysis of biomass particles, Journal of Analytical and Applied Pyrolysis 81 (2) (2008) 183–192. doi:https://doi.org/10.1016/j.jaap.2007.11.007.
URL https://www.sciencedirect.com/science/article/pii/S0165237007001532

[29] T. Fateh, T. Rogaume, F. Richard, Multi-scale modeling of the thermal decomposition of fire retardant plywood, Fire Safety Journal 64 (2014) 36–47. doi:10.1016/j.firesaf.2014.01.007.
URL https://linkinghub.elsevier.com/retrieve/pii/S0379711214000186

[30] S. Papari, K. Hawboldt, A review on the pyrolysis of woody biomass to bio-oil: Focus on kinetic models, Renewable and Sustainable Energy Reviews 52 (2015) 1580–1595. doi:10.1016/j.rser.2015.07.191.
URL https://linkinghub.elsevier.com/retrieve/pii/S1364032115008382

[31] J. Colombiano, B. Batiot, V. Dréan, F. Richard, E. Guillaume, T. Rogaume, Numerical analysis of the characteristics of the decomposition zone of a burning wood sample under cone calorimeter and evaluation of the limiting process, Journal of Analytical and Applied Pyrolysis 168 (2022) 105752. doi:https://doi.org/10.1016/j.jaap.2022.105752.
URL https://www.sciencedirect.com/science/article/pii/S0165237022003229

[32] B. Moghtaderi, V. Novozhilov, D. Fletcher, J. H. Kent, An Integral Model for the Transient Pyrolysis of Solid Materials, Fire Mater. 21 (1) (1997) 7–16. doi:10.1002/(SICI)1099-1018(199701)21:1<7::AID-FAM588>3.0.CO;2-T.
URL https://onlinelibrary.wiley.com/doi/10.1002/(SICI)1099-1018(199701)21:1<7::AID-FAM588>3.0.CO;2-T

[33] M. A. Masmoudi, M. Sahraoui, N. Grioui, K. Halouani, 2-D Modeling of thermo-kinetics coupled with heat and mass transfer in the reduction zone of a fixed bed downdraft biomass gasifier, Renewable Energy 66 (2014) 288–298. doi:10.1016/j.renene.2013.12.016.
URL https://linkinghub.elsevier.com/retrieve/pii/S0960148113006939

[34] A. Anca-Couce, G. Caposciutti, T. Gruber, J. Kelz, T. Bauer, C. Hochenauer, R. Scharler, Single large wood log conversion in a stove: Experiments and modelling, Renewable Energy 143 (2019) 890–897. doi:10.1016/j.renene.2019.05.065.
URL https://linkinghub.elsevier.com/retrieve/pii/S0960148119307256

[35] T. Kashiwagi, T. Ohlemiller, K. Werner, Effects of external radiant flux and ambient oxygen concentration on nonflaming gasification rates and evolved products of white pine, Combustion and Flame 69 (3)

(1987) 331–345. doi:10.1016/0010-2180(87)90125-8.
URL https://linkinghub.elsevier.com/retrieve/pii/0010218087901258

[36] J. D. Swann, Y. Ding, M. B. McKinnon, S. I. Stoliarov, Controlled atmosphere pyrolysis apparatus ii (capa ii): A new tool for analysis of pyrolysis of charring and intumescent polymers, Fire Safety Journal 91 (2017) 130–139.

[37] C. Lautenberger, C. Fernandez-Pello, Generalized pyrolysis model for combustible solids, Fire Safety Journal 44 (6) (2009) 819–839. doi:10.1016/j.firesaf.2009.03.011.
URL https://linkinghub.elsevier.com/retrieve/pii/S0379711209000332

[38] F. Jia, E. R. Galea, M. K. Patel, Numerical simulation of the mass loss process in pyrolizing char materials, Fire Mater. 23 (2) (1999) 71–78. doi:10.1002/(SICI)1099-1018(199903/04)23:2<71::AID-FAM672>3.0.CO;2-5.
URL https://onlinelibrary.wiley.com/doi/10.1002/(SICI)1099-1018(199903/04)23:2<71::AID-FAM672>3.0.CO;2-5

[39] F. Richter, G. Rein, A multiscale model of wood pyrolysis in fire to study the roles of chemistry and heat transfer at the mesoscale, Combustion and Flame 216 (2020) 316–325. doi:https://doi.org/10.1016/j.combustflame.2020.02.029.
URL https://www.sciencedirect.com/science/article/pii/S0010218020300924

[40] S. I. Stoliarov, R. E. Lyon, Thermo-kinetic model of burning for pyrolyzing materials, Fire Safety Science 9 (2008) 1141–1152.

[41] L. Terrei, G. Gerandi, H. Flity, V. Tihay-Felicelli, Z. Acem, G. Parent, P.-A. Santoni, Experimental and numerical multi-scale study of spruce wood degradation under inert atmosphere, Fire Safety Journal 130 (2022) 103598. doi:10.1016/j.firesaf.2022.103598.
URL https://linkinghub.elsevier.com/retrieve/pii/S0379711222000765

[42] J. Gong, M. Zhang, Pyrolysis and autoignition behaviors of oriented strand board under power-law radiation, Renewable Energy 182 (2022) 946–957. doi:10.1016/j.renene.2021.11.032.
URL https://linkinghub.elsevier.com/retrieve/pii/S0960148121016013

[43] N. Grioui, K. Halouani, A. Zoulalian, F. Halouani, Thermogravimetric analysis and kinetics modeling of isothermal carbonization of olive wood in inert atmosphere, Thermochimica Acta 440 (1) (2006) 23–30. doi:10.1016/j.tca.2005.09.018.
URL https://linkinghub.elsevier.com/retrieve/pii/S0040603105005009

[44] V. Dhyani, T. Bhaskar, A comprehensive review on the pyrolysis of lignocellulosic biomass, Renewable Energy 129 (2018) 695–716. doi:https://doi.org/10.1016/j.renene.2017.04.035.
URL https://www.sciencedirect.com/science/article/pii/S0960148117303427

[45] K. Slopiecka, P. Bartocci, F. Fantozzi, Thermogravimetric analysis and kinetic study of poplar wood pyrolysis, Applied Energy 97 (2012) 491–497. doi:10.1016/j.apenergy.2011.12.056.
URL https://linkinghub.elsevier.com/retrieve/pii/S030626191100852X

[46] C. Di Blasi, Heat, momentum and mass transport through a shrinking biomass particle exposed to thermal radiation, Chemical Engineering Science 51 (7) (1996) 1121–1132. doi:https://doi.org/10.1016/S0009-2509(96)80011-X.
URL https://www.sciencedirect.com/science/article/pii/S000925099680011X

[47] G. Maschio, C. A. Koufopanos, A. Lucchesi, Pyrolysis, a promising route for biomass utilization, Bioresource Technology 42 (1992) 219–231.

[48] T. Hosoya, H. Kawamoto, S. Saka, Cellulose–hemicellulose and cellulose–lignin interactions in wood pyrolysis at gasification temperature, Journal of Analytical and Applied Pyrolysis 80 (1) (2007) 118–125. doi:https://doi.org/10.1016/j.jaap.2007.01.006.
URL https://www.sciencedirect.com/science/article/pii/S0165237007000125

[49] P. Girods, A. Dufour, Y. Rogaume, C. Rogaume, A. Zoulalian, Thermal removal of nitrogen species from wood waste containing urea formaldehyde and melamine formaldehyde resins, Journal of Hazardous Materials 159 (2) (2008) 210–221. doi:https://doi.org/10.1016/j.jhazmat.2008.02.003.
URL https://www.sciencedirect.com/science/article/pii/S0304389408002331

[50] E. Chornet, C. Roy, Compensation effect in the thermal decomposition of cellulosic materials, Thermochimica Acta 35 (3) (1980) 389–393. doi:https://doi.org/10.1016/0040-6031(80)87140-1.
URL https://www.sciencedirect.com/science/article/pii/0040603180871401

[51] L. Terrei, Z. Acem, V. Marchetti, P. Lardet, P. Boulet, G. Parent, In-depth wood temperature measurement using embedded thin wire thermocouples in cone calorimeter tests, International Journal of Thermal Sciences 162 (2021) 106686. doi:10.1016/j.ijthermalsci.2020.106686.
URL https://linkinghub.elsevier.com/retrieve/pii/S1290072920311352

[52] L. Valencia, Experimental and numerical investigation of the thermal decomposition of materials at three scales: application to polyether polyurethane foam used in upholstered furniture (11 2009).

[53] C. Lautenberger, C. Fernandez-Pello, Generalized pyrolysis model for combustible solids, Fire Safety Journal 44 (6) (2009) 819–839. doi:https://doi.org/10.1016/j.firesaf.2009.03.011.
URL https://www.sciencedirect.com/science/article/pii/S0379711209000332

[54] N. Grioui, K. Halouani, A. Zoulalian, F. Halouani, Thermochemical modeling of isothermal carbonization of thick wood particle – Effect of reactor temperature and wood particle size, Energy Conversion and Management 48 (3) (2007) 927–936. doi:10.1016/j.enconman.2006.08.003.
URL https://linkinghub.elsevier.com/retrieve/pii/S0196890406002366

[55] H. Wenzl, The chemical technology of wood, (1970).

[56] A. Anca-Couce, N. Zobel, Numerical analysis of a biomass pyrolysis particle model: Solution method optimized for the coupling to reactor models, Fuel 97 (2012) 80–88. doi:10.1016/j.fuel.2012.02.033.
URL https://linkinghub.elsevier.com/retrieve/pii/S0016236112001561

[57] M. Spearpoint, J. Quintiere, Predicting the piloted ignition of wood in the cone calorimeter using an integral model — effect of species, grain orientation and heat flux, Fire Safety Journal 36 (4) (2001) 391–415. doi:https://doi.org/10.1016/S0379-7112(00)00055-2.
URL https://www.sciencedirect.com/science/article/pii/S0379711200000552

[58] P. Koch, Specific heat of ovendry spruce pine wood and bark, Wood science (1968).

[59] W. Simpson, A. TenWolde, Physical properties and moisture relations of wood, Chapter 3 (1999) 2–1.

[60] T. Harada, T. Hata, S. Ishihara, Thermal constants of wood during the heating process measured with the laser flash method, J Wood Sci 44 (6) (1998) 425–431. doi:10.1007/BF00833405.
URL http://link.springer.com/10.1007/BF00833405

[61] M. Gupta, J. Yang, C. Roy, Specific heat and thermal conductivity of softwood bark and softwood char particlesâ˜†, Fuel 82 (8) (2003) 919–927. doi:https://doi.org/10.1016/S0016-2361(02)00398-8.
URL https://www.sciencedirect.com/science/article/pii/S0016236102003988

[62] W. J. Parker, R. J. Jenkins, C. P. Butler, G. L. Abbott, Flash Method of Determining Thermal Diffusivity, Heat Capacity, and Thermal Conductivity, Journal of Applied Physics 32 (9) (1961) 1679–1684. doi:10.1063/1.1728417.
URL http://aip.scitation.org/doi/10.1063/1.1728417

[63] C. A. Koufopanos, A. Lucchesi, G. Maschio, Kinetic modelling of the pyrolysis of biomass and biomass components, The Canadian Journal of Chemical Engineering 67 (1) (1989) 75–84. arXiv:https://onlinelibrary.wiley.com/doi/pdf/10.1002/cjce.5450670111, doi:https://

644 doi.org/10.1002/cjce.5450670111.
645 URL https://onlinelibrary.wiley.com/doi/abs/10.1002/cjce.5450670111

646 [64] A. K. Sadhukhan, P. Gupta, R. K. Saha, Modelling of pyrolysis of large wood particles, Bioresource
647 Technology 100 (12) (2009) 3134–3139. doi:https://doi.org/10.1016/j.biortech.2009.01.007.
648 URL https://www.sciencedirect.com/science/article/pii/S0960852409000315

649 [65] C. D. Blasi, Physico-chemical processes occurring inside a degrading two-dimensional anisotropic porous
650 medium, International Journal of Heat and Mass Transfer 41 (24) (1998) 4139–4150. doi:https://doi.
651 org/10.1016/S0017-9310(98)00142-2.
652 URL https://www.sciencedirect.com/science/article/pii/S0017931098001422

653 [66] M. G. Grønli, M. C. Melaaen, Mathematical model for wood pyrolysiscomparison of experimental mea-
654 surements with model predictions, Energy and Fuels 14 (2000) 791–800.

655 [67] B. M. Suleiman, J. Larfeldt, B. Leckner, M. Gustavsson, Thermal conductivity and diffusivity of wood,
656 Wood Science and Technology 33 (6) (1999) 465–473. doi:10.1007/s002260050130.
657 URL http://link.springer.com/10.1007/s002260050130

658 [68] H. Flity, Y. Jannot, T. Terrei, P. Lardet, V. Schick, Z. Acem, G. Parent, Thermal conductivity parallel
659 and perpendicular to fibers direction and thermal capacity measurements of eight wood species up to
660 160 °c, (submitted 2023).

661 [69] B. Babu, A. Chaurasia, Heat transfer and kinetics in the pyrolysis of shrinking biomass particle, Chemical
662 Engineering Science 59 (10) (2004) 1999–2012. doi:https://doi.org/10.1016/j.ces.2004.01.050.
663 URL https://www.sciencedirect.com/science/article/pii/S0009250904001113

664 [70] R. Mehrabian, S. Zahirovic, R. Scharler, I. Obernberger, S. Kleditzsch, S. Wirtz, V. Scherer, H. Lu,
665 L. L. Baxter, A cfd model for thermal conversion of thermally thick biomass particles, Fuel Processing
666 Technology 95 (2012) 96–108. doi:https://doi.org/10.1016/j.fuproc.2011.11.021.
667 URL https://www.sciencedirect.com/science/article/pii/S0378382011004085

668 [71] B. Fredlund, Modelling of heat and mass transfer in wood structures during fire, Fire Safety Journal
669 20 (1) (1993) 39–69. doi:10.1016/0379-7112(93)90011-E.
670 URL https://linkinghub.elsevier.com/retrieve/pii/037971129390011E

671 [72] S. Alves, J. Figueiredo, A model for pyrolysis of wet wood, Chemical Engineering Science 44 (12) (1989)
672 2861–2869. doi:https://doi.org/10.1016/0009-2509(89)85096-1.
673 URL https://www.sciencedirect.com/science/article/pii/0009250989850961

[73] M. Janssens, J. Wells, Thermo-physical properties for wood pyrolysis models, pacific timber engineering conference, in: Pacific timber engineering conference, Vol. 1, Timber Research and Development Advisory Council;, 1994, pp. 607–618.
URL https://www.tib.eu/de/suchen/id/BLCP%3ACN012856593

[74] V. Hankalin, T. Ahonen, R. Raiko, On thermal properties of a pyrolysing wood particle, in: Finnish-Swedish Flame Days 2009, January 28-29, 2009, Naantali, Finland, 2009, p. 16 p.